TAMPEREEN TEKNILLINEN YLIOPISTO
TAMPERE UNIVERSITY OF TECHNOLOGY

Lu Zhao

Adaptive Disconnection Based Brain Hemisphere Segmentation in MRI: Applications to Brain Asymmetry Studies

Julkaisu 902 • Publication 902

Tampere 2010

Tampereen teknillinen yliopisto. Julkaisu 902
Tampere University of Technology. Publication 902

Lu Zhao

Adaptive Disconnection Based Brain Hemisphere Segmentation in MRI: Applications to Brain Asymmetry Studies

Thesis for the degree of Doctor of Science in Technology to be presented with due permission for public examination and criticism in Tietotalo Building, Auditorium TB224, at Tampere University of Technology, on the 22nd of June 2010, at 12 noon.

Tampereen teknillinen yliopisto - Tampere University of Technology
Tampere 2010

ISBN 978-952-15-2392-2 (printed)
ISBN 978-952-15-2433-2 (PDF)
ISSN 1459-2045

Abstract

With the development of neuroinformatics, a number of large international databases of brain imaging data have been built by integrating images collected from multiple imaging centers or neuroscientific research institutes. This thesis aims to develop accurate, robust and automatic brain image analysis methods that can be applied to analyze the images contained in the large databases.

First a fully automatic algorithm, the *Adaptive Disconnection* method, was developed to segment the brain volume into the left and right cerebral hemispheres, the left and right cerebellar hemispheres and the brainstem in three-dimensional magnetic resonance images. Using the partial differential equations based shape bottlenecks algorithm cooperating with an information potential value clustering process, the method detects and cuts, first, the compartmental connections between the cerebrum, the cerebellum and the brainstem in the white matter domain, and then, the interhemispheric connections of the extracted cerebrum and cerebellum volumes. The modeling of partial volume effect is used to locate cerebrum, cerebellum and brainstem boundaries, and make the interhemispheric connections detectable. With the knowledge of the subject orientation in the scanner, the *Adaptive Disconnection* method can automatically adapt the variations in subject location and normal brain morphology in different images without the aid of stereotaxic registration. The method was evaluated with one simulated realistic database and three clinical databases. The evaluation results showed that the developed method is very accurate and can well tolerate the image noises and intensity non-uniformity. The *Adaptive Disconnection* method was applied to analyses of cerebral structural asymmetries in schizophrenia. The obtained results were consistent with previously reported observations and hypotheses of abnormal brain asymmetry in schizophrenia.

Furthermore, an automatic shape analysis method was developed based on the *Adaptive Disconnection* method for studying the Yakovlevian torque in three-dimensional brain magnetic resonance images by numerically modeling the interhemispheric fissure shape with polynomial surface and measuring its regional averaged and local curvature features. This shape analysis method can produce straightforward quantification and geometric interpretation of local and regional Yakovlevian torque.

Preface

The work presented in this thesis has been carried out in the Department of Signal Processing of Tampere University of Technology during 2006 - 2010. First of all, I want to express my sincere gratitude to my supervisor, Professor Ulla Ruotsalainen for inviting me to the Department of Signal Processing, and introducing me to the world of medical imaging and neuroscience. Her continuous encouragement and support have inspired me always along the way. I am greatly indebted to my another supervisor Jussi Tohka, PhD, for his excellent technical guidance, endless patience, and constant willingness to help me with various issues. Without him, this thesis would have never become possible.

The reviewers of this thesis, PhD Keon van Leemput and PhD Jean-François Mangin deserve heartfelt thanks for their careful reading and constructive comments.

I wish to thank Professor Jarmo Hietala and PhD Jussi Hirvonen, from Turku PET centre, for their fertile co-operation in preparing the joint publications, and for providing MRI data and counseling on the neurophysiology and anatomy for this work. I sincerely thank Sari Peltonen, Harri Pölönen, Antonietta Pepe, Uygar Tuna, Jukka-Pekka Kauppi, Jari A. Niemi and all the other past and present members of the M^{2}oBSI research group for providing me their assistance when I needed. I would also like to thank the staff of the Department of Signal Processing, and the coordinator of international education of Tampere University of Technology, Ms Ulla Siltaloppi, for their help in many practical and administrative matters during these years.

From March to July 2009, I worked at McConnell Brain Imaging Centre (BIC) at Montreal Neurological Institute, McGill University, Canada. I am grateful for Professor Alan Evans for inviting me to BIC. I thank my colleagues at BIC for sharing their know-how and for many discussions related to medical image analysis as well as to other issues.

I wish to express my greatest thanks to my family for their never-ending love and support. I also give my warmest thanks to my friends for their constant support during this research.

Lastly, I want to express my gratitude towards the organizations that have financially supported this work. These are the Academy of Finland, grant No. 129657, Finnish Centre of Excellence programme (2006 - 2011), Tampere Graduate School of Information Science and Engineering (TISE), Tuula and Yrjö Neuvon Foundation and Ulla Tuominen Foundation.

Tampere, June 2010 Lu Zhao

Supervisors: Jussi Tohka, PhD
Academy Research Fellow
Department of Signal Processing
Tampere University of Technology

Professor Ulla Ruotsalainen
Department of Signal Processing
Tampere University of Technology

Reviewers: Keon van Leemput, PhD
Martinos Center for Biomedical Imaging
Massachusetts General Hospital and Harvard Medical School
and
MIT Computer Science and Artificial Intelligence Laboratory

Jean-François Mangin, PhD
Neurospin
Institut dimagerie BioMédicale
Direction des Sciences du Vivant

Opponents: Professor Jussi Parkkinen
School of Computing
University of Eastern Finland

René Westerhausen, PhD
Department of Biological and medical Psychology
University of Bergen

Contents

List of publications

This thesis is based on the following publications. These are referred to in the text as [Publication x], where x is a roman numeral.

Publication-I L. Zhao, J. Tohka, and U. Ruotsalainen. Accurate 3D left-right brain hemisphere segmentation in MR images based on shape bottlenecks and partial volume estimation. In B.K. Ersboll and K.S. Pedersen, editors, *Proc. of 15th Scandinavian Conference on Image Analysis, SCIA07, Lecture Notes in Computer Science 4522*, pages 581 - 590, Aalborg, Denmark, Springer Verlag, June 2007.

Publication-II L. Zhao and J. Tohka. Automatic compartmental decomposition for 3D MR images of human brain. *Proc. of 30th Annual International Conference of the IEEE Engineering in Medicine and Biology Society, EMBC08*, pages 3888-3891, Vancouver, Canada, August 2008.

Publication-III L. Zhao, U. Ruotsalainen, J. Hirvonen, J. Hietala and J. Tohka. Automatic cerebral and cerebellar hemisphere segmentation in 3D MRI: adaptive disconnection algorithm. *Medical Image Analysis*, volume 14, number 3, pages 360 - 372, 2010.

Publication-IV L. Zhao, J. Hietala and J. Tohka. Shape analysis of human brain interhemispheric fissure bending in MRI. *Proc. of 12th International Conference on Medical Image Computing and Computer Assisted Intervention, MICCAI09, Lecture Notes in Computer Science 5762*, pages 216 - 223, London, United Kingdom, Springer Verlag, September 2009.

List of abbreviations

3D	Three-dimensional
AC	Anterior commissure
ADFI	Alzheimer’s Disease Neuroimaging Initiative
AFNI	Analysis of Functional NeuroImages
AI	Asymmetry index
ANIMAL	Automated non-linear image matching and anatomical labeling
BET	Brain Extraction Tool
BS	Brainstem
BSE	Brain Surface Extractor
CB	Cerebellum
CBB	Cerebellum+brainstem
CH	Cerebrum
CLASP	Constrained Laplacian Anatomic Segmentation using Proximity
CSF	Cerebrospinal fluid
DBM	Deformation-based morphometry
EM	Expectation maximization
FDR	False discovery rate
GM	Gray matter
ICBM	International Consortium for Brain Mapping
INU	Intensity non-uniformity
LPBA	LONI Probabilistic Brain Atlas
IPV	Information potential value
MAP	Maximum a posteriori
MNI	Montreal Neurological Institute
MRI	Magnetic resonance imaging
MSP	Mid-sagittal plane
MSS	Mid-sagittal surface
PC	Posterior commissure
PDE	Partial differential equation
PET	Positron emission tomography
POI	Point of interest
PVE	Partial volume effect
ROI	Region of interest
VBM	Voxel-based morphometry
WM	White matter

Chapter 1

Introduction

1.1 Neuroinformatics

The interdisciplinary field of neuroinformatics combines neuroscientific research with information science/technology to develop and apply advanced tools and approaches for understanding the structure and function of the brain [36]. This new established research field covers three primary areas:

1. tools and databases for managing and sharing neuroscientific data;
2. methods and tools for analyzing the data;
3. computational models of the nervous system and neural processes.

neuroscientific research aims to understand the structure, function, and development of the nervous system in health and disease. Such understanding requires the integration of huge amounts of heterogeneous and complex data collected at multiple levels of investigation [14]. A number of neuroscience databases have been built based on a variety of data types, such as descriptive and numerical data, postmortem brain sections or three-dimensional (3D) brain images. These databases provide information about gene expression, neurons, macroscopic brain structure, and neurological or psychiatric disorders. This thesis concentrates on the databases of 3D brain images conveying the macroscopic anatomical information of human brain. Presently, the anatomical information of human brain is usually noninvasively acquired using the magnetic resonance imaging (MRI). Databasing a large number of MR images of human brain is important to address the normal variation in brain morphology in wide populations, and to find the structural changes related to aging, development or mental disorders. For example, the Brain Development Cooperative Group (including more than ten imaging centers and biomedical and neuroscientific research institutes) [38] built a large, demographically balanced brain MRI/clinical/behavioral database for development research on normal brain. In

this project, six pediatric study centers acquired images of about 500 children, and a data coordinating center consolidated these images. In another project, dozens of medical imaging centers and neuroscientific research institutes, cooperating together, built an Alzheimer's Disease Neuroimaging Initiative (ADNI) database [100], by collecting and integrating MRI and positron emission tomography (PET) scans of approximately 800 subjects. This ADNI database is applied to identify neuroimaging and other biomarkers of the cognitive changes associated with mild cognitive impairment and Alzheimer's disease.

Besides the two examples, many more large brain imaging databases of diverse imaging modalities have been built for various biomedical and neuroscientific applications. Nevertheless, data only make sense in the context of tools [14]. The problem is raised of how to develop effective methods and tools to analyze these databases. The first requirement is accuracy [21], i.e. the analysis results need to be able to accurately convey the actual anatomical or functional information of the studied subjects. The accuracy of an analysis method in practice is always affected by variations (sometimes unpredictable) in its implementing environment, e.g. data damage, alteration or loss of functionality, even though it has been methodologically optimized. Robustness [21] refers to the capability to cope well with the variations. From above examples of brain imaging databases, it can be seen that the images contained in the databases are often from multi-scanner and multi-center origin, so that the images may greatly differ in scanning environments, acquisition protocols and image quality. Consequently, the requirement for the robustness of the corresponding brain image analysis techniques is especially high. Moreover, neuroinformatics also aims to integrate and analyze the experimental data and results reported in thousands of publications for improving existing theories about the brain. This requires that the analysis needs to be reproducible to enable comparison between results of different studies. Reproducibility [21] refers to the ability of a test or experiment to be accurately reproduced, or replicated, by someone else working independently.

The third major direction of neuroinformatics, i.e. the development of computational models of the nervous system and neural processes, is out of the scope of this thesis, thus we will not go to details about this aspect.

1.2 Automatic brain image analysis

Traditionally, brain images are qualitatively analyzed with visual examination to locate and identify tumors, stroke or other signs of problems for diagnosis. This kind of qualitative analysis is time- and labor-consuming, and the pro-

duced measurements are subjective. In addition, qualitative analysis is rather difficult to reproduce. Experiments have shown that any given radiologist is unlikely to precisely agree even with himself if asked to analyze the same scan a week or two later [7]. Currently, the focus of medical imaging based brain research is shifting from qualitative analysis to quantitative analysis, which can produce reproducible and objective measurements. Based on large databases, quantitative analysis can detect more subtle group effects or small longitudinal changes over time, which might be used as measures of development, aging or disease.

1.2.1 Brain image segmentation

Before extracting and analyzing the quantitative information for quantitative brain image analysis, image segmentation has to be conducted to delineate the structures or regions of interest in the image. This work, previously, was mostly completed by trained clinicians with manual or semi-manual methods. This task is more and more difficult as the size and number of images increase. Therefore, the brain image segmentation has a far greater cost compared with the subsequent computation and analysis of the structural measurements, which can be performed automatically based on the intensity and geometric information contained in the image. Thus, the major task to automate the brain image analysis is to automate the brain image segmentation.

In addition to saving time and labor, automatic image segmentation produces more reproducible results compared to manual segmentation, because automatic methods always work in the same way [151]. Automation of image segmentation also helps reduce errors caused by fatigue. These advantages of automatic image segmentation make predicting segmentation error or failure possible, so that the images containing artifacts that could lead to errors or failure but can not be compensated for can be discarded in advance.

Automation of brain image segmentation is rather complicated and difficult, because it is not possible using only the information available in the images. Different brain structures often have the same or very similar intensity values, and the subject morphology varies between different individuals. *A priori* anatomical knowledge of the spatial relationships between different brain structures has to be taken into account. Using high-level prior knowledge could simplify the segmentation problem, nevertheless, the complexity of the method would be increased and the robustness of the method would be degraded. Usually, a computerized brain atlas or pre-segmented brain template is utilized to assist in automatic brain image segmentation through stereotaxic image registration. In this way, the final segmentation accuracy would be sensitive to the

accuracy of the stereotaxic registration, which is affected by several factors, e.g. the choice of the algorithm and the template image used. Furthermore, employing image registration also would weaken the segmentation methods' robustness, because the available atlas or template may not be suitable to the processed data set. For example, an atlas of adult's brain can not be applied to process images of children. In practical application, the accuracy and robustness of automatic brain image segmentation methods are also challenged by the image noise and equipment-dependent artifacts, the levels of which vary between different scanners. Therefore, the automation of brain image segmentation is still one of the most studied topics in brain image analysis.

1.2.2 Brain anatomy analysis

After segmenting the brain volume in MRI, the simplest possibility to study brain anatomy is to analyze the global and regional volumes of the brain. For this purpose, the volumes of the studied subjects or the segmented subparts are computed, and the differences between two groups or the volume changes in the longitudinal studies are statistically analyzed. Volume analysis can detect global anatomic properties or variabilities, e.g. atrophy or dilation. However, local structural changes may be overlooked, because: two structures having equal volumes might have completely different shapes; and local shape variation does not necessary result in a detectable volume change. Additionally, the volume alone is not able to give a thorough description on the structure. Therefore, more detailed shape analysis is needed for more accurate understanding of the human brain and its changes, and to discover the shape changes related to certain factors of interest. Shape analysis provides complementary information that may improve results in many cases. Shape analysis may be particularly useful for examining subtle structural changes that do not manifest as volume variation of the whole structure. It should be emphasized that shape analysis is not intended to completely replace volume analysis.

1.3 Objectives and structure of the thesis

The objective of this thesis is to develop completely automatic 3D brain MR image analysis methods, which are able to serve the large databases based brain anatomy studies. First, we developed an *Adaptive Disconnection* method to segment the brain volume into the left and right hemispheres of the cerebrum (CH), the left and right hemispheres of the cerebellum (CB) and the brainstem (BS) in MRI. This method was applied to study structural asymmetries of hu-

man brain. Second, based on the *Adaptive Disconnection* method, an automatic shape analysis approach was developed to investigate the Yakovlevian torque of human brain by quantifying the interhemispheric fissure bending.

The principal brain MRI analysis approaches in the scope of this thesis, such as skull-stripping, intensity non-uniformity correction, brain tissue classification, partial volume modeling, spatial normalization, neuroanatomical segmentation and brain shape analysis, are introduced in Chapter 2. Automatic brain hemisphere segmentation techniques (to segment the left and right hemispheres of CH, the left and right hemispheres of CB and BS in 3D MRI) are reviewed in Chapter 3. With this review, the challenges and methodological restrictions are discussed. Chapter 4 gives description of the *Adaptive Disconnection* method and how the problems discussed in the above chapter were settled. Chapter 5 focuses on the applications of *Adaptive Disconnection* method to MRI based brain asymmetry studies. The major contributions of this thesis are summarized in Chapter 6. The methods and results presented in this thesis are discussed in Chapter 7.

Chapter 2

Brain MRI analysis

A procedure of automatic quantitative brain image analysis consists of the following principal steps: first, image quality improvement to compress the image noise and artifacts; second, image segmentation to delineate the structures or regions of interest; third, spatial normalization with stereotaxic image registration; forth, quantitative information extraction and statistical analysis or comparison between populations. It should be noted that these steps, especially image segmentation and spatial normalization, could be arranged in different order for different analysis algorithms or for different investigation purposes. It is also possible to use a single framework to simultaneously produce joint solutions for image quality improvement, image segmentation and spatial normalization, e.g. Ashburner and Friston's unified segmentation algorithm [5]. Fig.2.1 illustrates the brain MRI analysis pipeline used in this thesis. In this chapter, the brain MRI analysis techniques related to the work proposed in this thesis are introduced.

Figure 2.1: Automatic brain MRI analysis pipeline used in this thesis.

2.1 Skull-stripping

Quantitative morphometric studies of brain MRI often require a preliminary step to isolate brain from extracranial or 'nonbrain' tissues. This preliminary

step is commonly referred to as skull-stripping [40]. Numerous automatic skull-stripping methods have been developed and widely used, which are based on the signal intensity and signal contrast in the MR image. Thresholding based methods define minimum and maximum values along the axis representing voxel intensity histogram (e.g. [32]). Multivariate histograms are used when a study collects images with varying contrast. Morphology or region-based methods (e.g. 3dIntracranial in the Analysis of Functional NeuroImages (AFNI) software package [27]), cooperated with intensity thresholding methods, use connectivity between regions, such as similar intensity values. Skull-stripping in MRI can also be obtained by cooperating morphological methods with edge detection [e.g. Brain Surface Extractor (BSE) [113] in the BrainSuite software package [118]]. Watershed algorithms try to find a local optimum of the intensity gradient for preflooding of the defined basins to segment the image into brain and nonbrain components (e.g. [50]). Surface-model-based methods extract the brain volume through modeling the brain surface with a smoothed deformed template [e.g. the FreeSurfer software package [30], Brain Extraction Tool (BET) [122]]. A recent Hybrid Watershed method [116] was developed by incorporating the watershed techniques with the surface-model-based methods to locate the brain boundary in MRI.

2.2 Intensity non-uniformity correction

One of the major artifacts affecting the results of automatic quantitative brain MRI analysis is the intensity non-uniformity (INU), which refers to the phenomenon of nonuniform tissue intensities in the images [121] (see Fig.2.2). INU has no anatomical relevance, and for MRI it is due to the combined effect of the imaged subject, the MR pulse sequence and the imaging coils. Therefore, MR physicists correct INU in MRI by improving the image acquisition protocol with the prior knowledge about these factors [9].

Differently, image processing specialists correct INU in MR images by using numerous methods based on some assumptions regarding the acquisition process. Such as, correction algorithms based on the grayscale spatial distribution rely on the assumption that the variation of INU is spatially smooth and slowly varying across the image and that the ideal image is piecewise constant. In this way, some methods model INU as a smooth surface using spline [31, 73, 160] or polynomial [97, 125, 135] basis functions, and then the correction is conducted by dividing the corrupted image by the fitted surfaces. Some other methods employing low-pass filtering [53, 67, 101, 141, 159] or homomorphic filtering [19, 47, 60] first extract INU as a signal consisting of

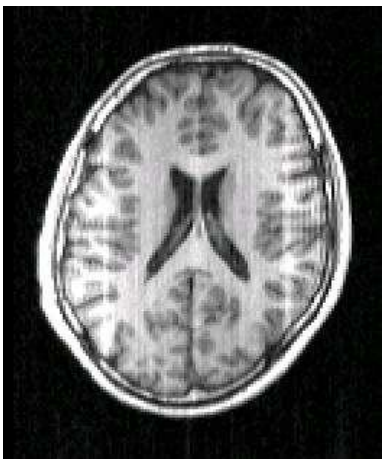

Figure 2.2: Example of intensity non-uniformity in MR brain image. The intensities of the white matter at the left and right sides are notably higher than other white matter area.

low spatial frequency intensity variation and then divide the corrupted data by the extracted INU for correction. Besides in the spatial domain, INU correction can also be achieved in other domains [9], such as the Fourier domain [24, 143], the wavelet domain [52, 83], and the probability density functions domain [81, 90, 98, 120, 123, 142]. In the Fourier domain, INU is corrected by applying the low-pass gaussian filters. In the wavelet domain, the corrupted image is first decomposed into a cascade of orthogonal approximation subspaces containing low-frequency information and detail subspaces containing high-frequency information for different spatial resolutions. Next, INU is estimated and corrected in the approximation subspaces. In the probability density functions domain, INU is considered as a convolution term smoothing the real intensity distribution and increasing entropy. Thus, INU can be corrected with an entropy minimization framework. Moreover, it is also very typical to find a joint solution to both brain tissue classification and INU correction with statistical methods, e.g. the Expectation-Maximization (EM) based [139, 140, 147] or fuzzy *c*-means clustering [106] based methods.

2.3 Brain tissue classification and partial volume modeling

Brain tissue classification in 3D MRI is to classify and label the voxels in a brain image as belonging to one of the three primary tissue types: gray matter (GM), white matter (WM) and cerebrospinal fluid (CSF), according to certain

criteria. This process is important for multi-modality image correlation, visualization, and quantification, and clinical uses such as tumor and lesion detection [111]. Brain tissue classification in MRI can be obtained using thresholding based techniques [61, 70, 82, 127], which attempt to determine a threshold value that separates the desired tissue types. However, thresholding based approaches are very sensitive to image noise and artifacts. Currently, statistical classification based algorithms [33, 56, 109, 139, 140, 147], which are more robust and have rigorous mathematical foundations in stochastic theory, have been widely applied. In these methods, the probability density functions of tissue intensity for different tissue classes are parametrically modeled as one or more Gaussian mixtures. EM algorithm is often used to estimate the model parameters, and Markov random field is usually employed to model the spatial interactions between neighboring voxels. Another major class of brain tissue classification techniques uses clustering-based methods, e.g. the fuzzy *c*-means clustering algorithms [11, 17, 51, 80, 106]. The clustering-based methods attempt to classify a voxel to a tissue type by using the notion of similarity to the tissue type.

Most of the above discussed methods produce only hard classification between GM, WM, and CSF. However, due to the existence of the partial volume effect (PVE), i.e. a single voxel can contain multiple tissue types due to finite image resolution (see Fig.1 in [Publication III]), labeling a voxel as just a single tissue type can not reveal all possible information about the tissue content of that voxel [137]. This can be problematic in small structures or highly convoluted areas of the brain. The fuzzy *c*-means clustering algorithm allows partial membership in different tissue classes. Thus, it can be used to model PVE, e.g. in [17, 106]. The most commonly used, statistically based model of PVE is the mixel model proposed by Choi et al. in [22]. This mixel model assumes that the intensity value of each voxel in the brain image is a realization of a weighted sum of random variables each of which characterizes a pure tissue type. Based on the mixel model or a closely related model without trying to estimate the weighting parameters, some methods [74, 111, 114] were developed to classify the voxels contained in MR brain volumes into not only the pure tissue types but also their mixures (GM/WM, GM/CSF and CSF/background). This kind of voxel labeling concerning the partial volume mixtures is called partial volume voxel classification. Estimating the amount of each brain tissue types contained in each voxel is called partial volume estimation. It provides more interesting information than merely identifying voxels containing PVE for many neuroscientific studies, e.g. cortical surface extraction [1, 64]. Partial volume estimation methods based on the mixel model [103, 118, 137] obtain the fractional content of each brain tissue type in each voxel by estimating the weighting parameter

with maximum-likelihood estimation.

2.4 Spatial normalization

Spatial normalization of brain images refers to the stereotaxic image registration process to transform individual images to match a standard brain template. In quantitative brain MRI analysis, spatial normalization is often applied to compensate for the subject movement, inter-image differences in voxel size and image resolution, or to build reliable spatial correspondences of homologous areas between individuals. Sometimes to assist brain neuroanatomical segmentation, spatial normalization is also employed to compensate for the variations in subject's location and morphology, and consequently to make the employed *a priori* anatomical knowledge applicable for the segmentation problem.

In general, there are two kinds of image registration used for spatial normalization: linear and nonlinear registration. A 3D linear registration, including rigid (only rotations and translations) and affine transformation (rotations and translations as well as stretches and shears), can be described with a 4×4 constant transformation matrix as

$$\begin{bmatrix} \beta_1 \\ \beta_2 \\ \beta_3 \\ 1 \end{bmatrix} = \left[\begin{array}{ccc|c} & A & & t \\ \hline 0 & 0 & 0 & 1 \end{array}\right] \begin{bmatrix} \alpha_1 \\ \alpha_2 \\ \alpha_3 \\ 1 \end{bmatrix}, \tag{2.1}$$

where $\alpha = [\alpha_1, \alpha_2, \alpha_3]^T$ and $\beta = [\beta_1, \beta_2, \beta_3]^T$ are the coordinate vectors in the original and transformed images respectively, A is the composition of the rotation, stretch and shear matrices, t is the translation vector. Nonlinear registration (nonrigid or elastic transformation), can not be represented using constant matrices. Most applications represent nonlinear transformations in terms of a local vector displacement field:

$$\beta_i = \alpha_i + T_i(\alpha), \tag{2.2}$$

where i = 1, 2 or 3 in 3D, $T_i(\alpha)$ is the displacement function for the ith coordinate with respect to the original coordinates, or as polynomial transformations in terms of the original coordinates.

A simple possibility to compute the registration parameters for spatial normalization is to use volume-matching algorithms, such as the Talairach proportional grid normalization [128], which use manually identified landmarks to find the best scaling parameters. Current automatic image-matching algorithms

[132] use a mathematical measure of overall image mismatch and a minimization algorithm with iterative changes in transformations to find the best set of transformations to match the image to the template. These methods usually first optimize linear transformation parameters (translations, rotations, stretches and often shears), and then find the best set of nonlinear warping parameters to further match the detail of brain shape [3, 115, 149]. Sulcal-matching methods [42, 43, 132, 134] attempt an explicit match of sulcal anatomy between subjects. In this type of methods, first a model of the cortical surface is extracted from the image, then the model of the cortical surface is distorted to match it with the template.

2.5 Neuroanatomical segmentation

Automatic neuroanatomical segmentation of brain image refers to the delineation of structures or regions of interest in certain brain tissue types. This is a comprehensive issue. Different approaches and *a priori* anatomical knowledge are required for the segmentation of different neuroanatomical regions. The methods for segmenting the left and right hemispheres of CH, the left and right hemispheres of CB and BS in 3D MRI (this segmentation is named 'brain hemisphere segmentation' in the following context), which is the concentration of this thesis, will be reviewed in the next chapter in detail. Here, the existing techniques for the segmentation of other neuroanatomical structures or regions of interest, such as the cerebral cortical subdivisions and subcortical structures (hippocampus, caudate, putamen and lateral ventricles), are briefly introduced.

A popular approach to obtain the segmentation of brain neuroanatomical substructures in 3D MR images is to use atlas deformation. For example, the automated nonlinear image matching and anatomical labeling (ANIMAL) algorithm [25] labels brain voxels as distinct structures by deforming one MRI volume to match another previously parcellated MRI template volume. It builds up the 3D nonlinear deformation field in a piecewise linear fashion, fitting cubical neighborhoods in sequence. The accuracy of atlas deformation based segmentation methods is limited by diverse types of error. These errors include inaccuracies of the atlas used as a starting point, errors in the registration process, and localized failure of the assumption of the inter-subject correspondence. Resently, it has been realized that the accuracy of atlas deformation based segmentations can be improved by registering a single image with multiple atlases. The multiple-atlas deformation based approaches (e.g. [55, 65]) combine segmentations obtained based on a set of single atlases using a suitable decision fusion algorithm. In this way, the resulting fused segmentation

can be more accurate than any of the single segmentation as random errors tend to cancel each other out in the combination.

The 3D segmentation problem can also be solved with a maximum a posteriori (MAP) framework in which both appearance (voxel intensities) models and shape (geometry) priors are defined [138]. Often, either a generative or a discriminative model is used for the appearance model, while the shape models are mostly generative based on either local or global geometry. Once an overall target function is defined, different methods, such as Iterated Conditional Modes algorithm [41], the variational method [138, 153], EM [107], Markov Chain Monte Carlo [34, 150], are then applied to find the optimal segmentation.

2.6 Brain shape analysis

Currently, the interest of brain anatomy study has been transferred from the global or regional volume measurements based analysis to more complicated shape analysis. Based on MRI, global shape indices measuring the sphericity [78], the cross-sectional area [152], surface area and depth of the object of interest [92] have been applied to reveal information on the global shape variabilities of human brain. Nevertheless, they do not give information on the location of the shape changes.

The progress in brain atlases and high-dimensional mapping have enabled the accurate local computational analysis of the brain structures [133]. Voxel-based morphometry (VBM) [4] aligns the brain images into the same coordinate system to obtain the voxel correspondence, and then analyzes the distributions of the brain tissue classes (GM, WM and CSF) in each voxel within or between groups. The geometric properties of human brain can be analyzed with the deformation-based morphometry (DBM). The voxel-wise correspondence is established using nonlinear registration, and the resulting deformation fields are used to analyze the inter-subject brain differences. The deformation fields [131], their parameters [6], or features computed from the norm, divergence, and Jacobian determinant of the deformation fields [45, 130] provide information on the local shape and volume changes. Techniques based on either VBM or DBM are usually employed to study the whole brain, and the analysis is not focused on any particular brain structure.

To acquire measurements of the local shape of brain, the shape representations of brain and its substructures can be modeled with deformable surface meshes [99]. Detailed shape analysis of a particular brain structure is conducted by utilizing the correspondence between the shape representations, which is

mostly obtained using high-dimensional mapping [16, 23, 29, 66, 133]. After the correspondence is found, the signed distances or differences of shape measurements between the studied shape and the reference shape or the subject pair are utilized to quantify the shape difference at each vertex (voxel on surface) [46, 66, 76, 129].

Chapter 3

Brain hemisphere segmentation

3.1 Introduction

Three primary anatomical subdivisions of human brain are CH, CB and BS. CH is the largest subdivision of human brain and associated with higher brain function such as thinking, language, action, motor, vision and etc. CB, located in the inferior posterior portion of the head, associated with regulation and coordination of movement, posture, and balance of human body. BS is the lower part of human brain, and provides the main motor and sensory innervation to the face and neck via the cranial nerves. Due to the anatomic and functional differences, CH, CB and BS are always studied separately in neuroscience. Furthermore, hemisphere segmentation of CH and CB is important for brain asymmetry studies, which can reveal the evolutionary, hereditary, developmental and pathological information of human brain. Hemisphere segmentation is also needed to view the medial surface of the cerebral hemispheres, because many important brain structures, such as the medial temporal lobe, cingulum, and large portions of the frontal, parietal and occipital lobes, can be only viewed in the interhemispheric medial surface.

The procedure of brain hemisphere segmentation into the left and right CH, left and right CB, and BS in MRI consists of two principal steps: 1) extracting the brain volume, and 2) segmenting the structures of interest. To extract the brain volume, first, nonbrain tissues are removed from the whole head MR image through skull-stripping (see Section 2.1). Next, brain tissue classification (see Section 2.3) is conducted to classify the voxels contained in the skull-stripped volume into GM, WM and CSF. Finally, the brain volume is extracted as the aggregation of the GM and WM voxels.

The automatic segmentation between the left and right CH, left and right

CB, and BS in the extracted brain volume can be achieve by using either the segmentation-surface-searching or structure-reconstruction based techniques. The existing techniques are discussed in the following sections in detail.

3.2 Segmentation surface searching

Because normal human brains exhibit an approximate bilateral symmetry with respect to the interhemispheric (longitudinal) fissure bisecting the brain, a simple way to segment the two brain hemispheres is to detect the longitudinal median plane of the brain, known as the mid-sagittal plane (MSP). MSP can be found as either the plane best matching the interhemispheric fissure [20, 95], or the plane maximizing the bilateral symmetry [84, 108, 126]. MSP can also be extracted in MR brain images by using the linear stereotaxic registration [18]. Images of different subjects are linearly transformed to match a symmetric brain template then the longitudinal median plane of the stereotaxic space is the wanted MSP. The validity of the MSP based brain hemisphere segmentation is based on the assumption of brain symmetry. However, in fact, human brain is never absolutely symmetric, and the interhemispheric boundary is actually a curved surface. Therefore, MSP is not able to segment the brain hemispheres accurately no matter how well it is extracted (see Fig.3.1-a). This inherent lim-

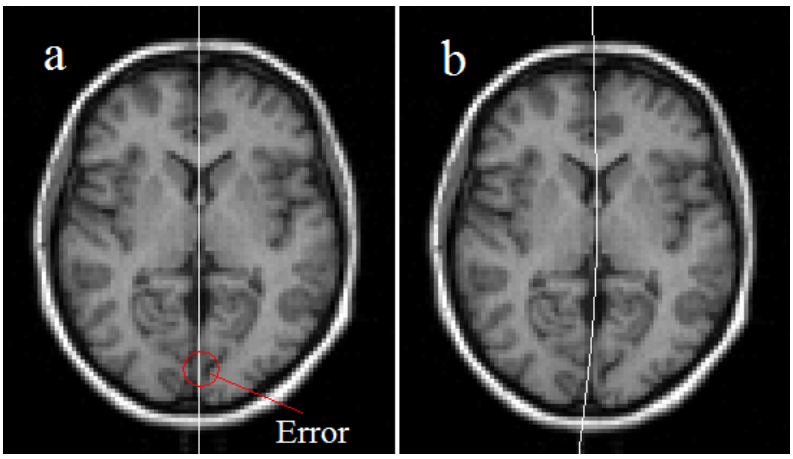

Figure 3.1: Brain hemisphere segmentation with MSP (a) and MSS (b) in MRI. MSP was generated using the linear stereotaxic registration, MSS was obtained by transforming the MSP in (a) using nonlinear registration. Both MSP and MSS are visualized as longitudinal lines in the transverse view. Visible segmentation error for MSP is highlighted in the red circle in (a).

itation of MSP has been qualitatively and quantitatively demonstrated in [Publication I and III].

For more accurate brain hemisphere segmentation, a simple way is to transform MSP into a curved mid-sagittal surface (MSS). Nonlinearly registration can be utilized for this purpose: a symmetric brain template is nonlinear registered into a specific brain image, and then MSP of the template is transformed into MSS using the transformation parameters estimated in the nonlinear registration. The nonlinear registration based MSP transformation was validated for brain hemisphere segmentation in [Publication III]. Compared with MSP, the transformed MSS could increase the hemisphere segmentation accuracy remarkably (see Fig.3.1-b).

Like MSP, the nonlinearly transformed MSS is not, in itself, able to separate CH, CB and BS. This problem can be solved with registration-morphing-based methods [75, 89], which nonlinearly transform the compartment outlines in a pre-segmented brain template into the images of specific subjects.

The ventricles, interhemispheric fissure and the gaps between CH and cerebellum+brainstem (CBB) are filled with CSF. Another scheme to detect surfaces separating left and right CH and CBB in MRI is to extract a membrane in the CSF-filled space, which follows the brain surface but does not penetrate sulci to any great extent (see Fig. 3.2). With image intensity based opti-

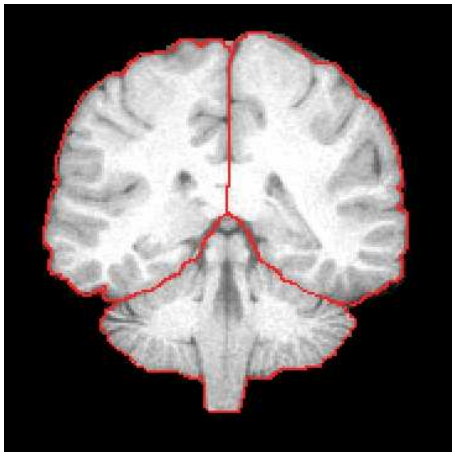

Figure 3.2: Membrane through the CSF-filled space separating left and right CH and CBB.

mization criteria, Marais et al. [94] used a constrained mesh surface to iteratively approximate the brain boundary, and Liang et al. [79] utilized the graph cuts algorithm to locate the segmentation surfaces. An inherent problem for segmentation-surface-searching based techniques is the compartmental uncertainty, i.e. a voxel at the segmentation boundary can belong to more than one structures.

3.3 Compartmental structure reconstruction

Another type of brain hemisphere segmentation techniques is to first find seed voxels corresponding to the wanted hemispheric compartments and then reconstruct their structures (surfaces or volumes) from the seed voxels towards the structure boundaries (CSF-GM interface) (see Fig.3.3). The region of WM is

Figure 3.3: Brain compartment segmentation using structure reconstruction from seed voxels. Left: initial state (compartmental seeds). Middle: intermediate state. Right: final state (reconstructed compartments).

mostly employed as the seed source. It can be segmented with two cutting planes as in FreeSurfer [30] and BrainVoyager [68] software packages: one sagittal plane across the corpus callosum to separate the left and right CH, and one horizontal plane through the midbrain or upper pons separating CH from CBB. The Constrained Laplacian Anatomic Segmentation using Proximity (CLASP) package [64] first extracts the CH volume with a stereotaxic CH mask, then segments the left and right CH in WM with MSP passing through the anterior and posterior commissures (AC and PC). The more complex morphology of the connections between CB and BS can not be addressed by cutting planes. BrainVisa software package [93] utilized the morphological erosion to disconnect the left and right CH and CBB in the WM volume. Hata et al. [54] found the compartmental seeds throughout the brain domain with fuzzified anatomical location knowledge of left and right CH, CB and BS. Both of these two algorithms can be extended to segment CBB into CB hemispheres and BS in WM area.

With compartmental seeds, the final segmentations are obtained by reconstructing the compartment structures. FreeSurfer [30] completes this by deforming the surfaces of the segmented WM compartments to follow the intensity gradients between GM and CSF (the pial surface). BrainVoyager [68] reconstructs the cortical surface by shifting each vertex on the WM compartments' surfaces along its surface normal until its position coincides with the

respective intensity contour of GM outer boundary. CLASP [64] deforms the WM surfaces of the compartments to the cortical surface along a Laplacian field between the WM surfaces and the skeletonized CSF fraction. The compartment shape reconstruction can also be achieved by reconstructing the volumes of the target compartments. In this way, a generalized Voronoï diagram is produced, from which compartmental segmentation can be obtained directly. BrainVisa [93] conditionally dilates the eroded WM mask to reconstruct the volumes of the left and right CH and CBB. Hata et al. [54] reconstructed volumes of the left and right CH, CB and BS from the seed voxels using a region growing algorithm based on the fuzzified compartment boundary location and intensity knowledge.

3.4 Challenges and methodological limitations

Both the segmentation-surface-searching based and structure-reconstruction based techniques confront difficulties to identify compartment boundaries when they are blurred by PVE. In MR brain images, there exist three types of PVE mixtures: CSF/GM, GM/WM, and CSF/background. These PVE mixtures, especially CSF/GM, blur the boundaries of the compartments of interest, e.g. the interface between CH and CB that in practice is a thin CSF area. This boundary blurring caused by PVE decreases the accuracy of boundary detection with the boundary intensity based optimization criteria for segmentation-surface-searching based techniques; and brings difficulties to locating the CSF-GM interface for restricting the structure reconstruction for the structure-reconstruction based methods. Currently, the problem of boundary blurring caused by PVE has been noticed and addressed in cortical surface extraction for cortex shape analysis [1, 64]. However, to our knowledge, CLASP [64] is the only approach explicitly model PVE among the existing brain hemisphere segmentation methods, which guides the cortical surface reconstruction with a skeletonized partial volume CSF surface rather than with the CSF-GM interface. The skeletonized partial volume CSF surface is obtained by skeletonizing all the voxels purely or partially containing CSF using a 2-subfield connectivity-preserving medial surface skeletonization algorithm [87].

As discussed in previous chapter, *a priori* anatomical knowledge of the spatial relationships between the compartments of interest has to be taken into account for automatic segmentation. However, the automatic segmentation based on the *a priori* anatomical knowledge could not be directly applied to MR brain images in native spaces due to the variations in brain location and morphology in different images. Therefore stereotaxic registration based spatial normaliza-

tion is needed to address this problem. Segmentation-surface-searching based methods [79, 94] use affine transformation to register processed images with a standard brain template to obtain initial location of the detected segmentation surfaces. Structure-reconstruction based methods [30, 64, 68] register subject volumes into standard Talairach coordinates [128] to locate the cutting planes for initial segmentation in WM area. BrainVisa [93] uses registration with a pre-segmented brain template to control the erosion size. The fuzzy logic based method [54] needs the subject spatial normalization to ensure the applicability of the fuzzified anatomical location knowledge for the target structures. Although the stereotaxic registration based spatial normalization is not the core of the segmentation algorithms, the final segmentation accuracy is sensitive to the accuracy of the stereotaxic registration, which is affected by several factors, e.g. the choice of the algorithm and the template image used. Moreover, employing image registration also reduces the methods' robustness.

In addition, effective techniques have been developed for denoising [112] and INU correction (see Section 2.2) in MRI. Nevertheless the image noise and INU are still potential challenges for automatic brain image segmentation when they are too severe to correct, because most of the existing segmentation approaches and the employed image registration algorithms are based on voxel intensities. For example, in [Publication III], it was demonstrated that the nonlinear MSS extraction method and BrainVisa were sensitive to noise and INU. Furthermore, most of the existing brain hemisphere segmentation methods are not able to separate BS from CB, because the complex morphology of the connections between CB and BS can not simply be addressed by cutting planes, and image intensity can not provide sufficient information to locate the segmentation boundaries between CB and BS.

Chapter 4

Adaptive Disconnection method

In this thesis, we developed a novel automatic brain hemisphere segmentation method, named *Adaptive Disconnection*. Based on the partial differential equations (PDE) based shape bottlenecks algorithm [91], this method detects and cuts the connections between the left and right CH, the left and right CB and BS in 3D brain MRI. Partial volume modeling is used to address the compartment boundary blurring caused by PVE, and to make the interhemispheric connections detectable. When the subject orientation in the scanner is known, this algorithm can automatically adapt the brain volume in the native space so that no spatial normalization is needed. In this chapter, the methodological details and evaluations of the *Adaptive Disconnection* method are introduced.

4.1 Shape bottlenecks algorithm

To detect and cut the connections between the left and right CH, the left and right CB, and BS in 3D brain volume, we utilized the PDE based shape bottlenecks algorithm proposed by Mangin et al. [91]. The essence of the PDE based shape bottlenecks algorithm is an application of Laplace's equation. Laplace's equation is a second-order PDE for a scalar field i that is enclosed between boundaries H and L. The mathematical form of Laplace's equation in 3D Cartesian coordinates is

$$\triangle i = \frac{\partial^2 i}{\partial x^2} + \frac{\partial^2 i}{\partial y^2} + \frac{\partial^2 i}{\partial z^2} = 0, \tag{4.1}$$

where $\triangle$ refers to the Laplace operator. An important property of Laplace's equation that underlines geometric structure is that Laplace's equation describes a layered set of nested surfaces that make a smooth transition from H to L [62]. Due to this property, Laplace's equation have been presently applied to

extract the pail surface by expanding the GM-WM surface [64] and to compute the cortical thickness [1, 62, 110, 156]. Differently from these applications to cortical surface shape analysis, the PDE based shape bottleneck algorithm uses Laplace's equation to detect the shape bottlenecks[1] between two parts of a complex 3D object Θ by simulating the steady state of an information transmission process between them.

Denote the boundary of Θ by Ω. In the PDE based shape bottlenecks algorithm, the simulated information is supposed to be transmitted from a boundary subset $H \subset \Omega$ towards another boundary subset $L \subset \Omega$ (see Fig. 4.1-a). The propagated information is quantified as information potential values (IPV). The information source H and terminal L are defined with the Dirichlet boundary condition:

$$\forall \mathbf{z} \in H \quad i(\mathbf{z}) = h\,; \quad \forall \mathbf{z} \in L \quad i(\mathbf{z}) = l\,, \tag{4.2}$$

where $\mathbf{z}$ is a voxel in Θ, $i(\mathbf{z})$ is the IPV at $\mathbf{z}$, h and l are constant IPVs, $h > l$. The rest of the boundary $(\Omega - (H + L))$ is defined with the Neumann boundary condition that is much more complicated. Additionally, the information transmission process inside Θ is assumed to have a conservative flow, and the interior region of Θ can be modeled as a Laplace's equation (Eq.4.1). By discretizing Eq.4.1, the consistent second order discrete Laplace's equation is obtained for Θ interior as

$$\begin{aligned} &\frac{1}{\delta_x^2}\big[i(x-1,y,z) - 2i(x,y,z) + i(x+1,y,z)\big] \\ +&\frac{1}{\delta_y^2}\big[i(x,y-1,z) - 2i(x,y,z) + i(x,y+1,z)\big] \\ +&\frac{1}{\delta_z^2}\big[i(x,y,z-1) - 2i(x,y,z) + i(x,y,z+1)\big] = 0, \end{aligned} \tag{4.3}$$

where $i(x, y, z)$ is the IPV at point $(x, y, z) \in (\Theta - \Omega)$, and δ_x, δ_y, δ_z correspond to voxel dimensions in x, y and z directions. Solving Eq.4.3 gives IPV of each voxel inside Θ:

$$\begin{aligned} i(x,y,z) = \frac{1}{2(\frac{1}{\delta_x^2} + \frac{1}{\delta_y^2} + \frac{1}{\delta_z^2})} \times \Big\{ &\frac{1}{\delta_x^2}\big[i(x-1,y,z) + i(x+1,y,z)\big] \\ &+ \frac{1}{\delta_y^2}\big[i(x,y-1,z) + i(x,y+1,z)\big] + \frac{1}{\delta_z^2}\big[i(x,y,z-1) \\ &+ i(x,y,z+1)\big]\Big\}, \end{aligned} \tag{4.4}$$

[1] Shape bottlenecks refer to the bridge-like connections between different compartments of a complex object.

The steady state of the simulated information transmission process is acquired by implementing a successive over relaxation iterative scheme [91]. When the simulated information transmission process converges, the two parts of Θ will have high gradients of IPV, and the shape bottlenecks connecting them will have median IPVs (see Fig.4.1-b). Simply clustering IPV would produce compartmental segmentation at the shape bottlenecks (see Fig.4.1-c).

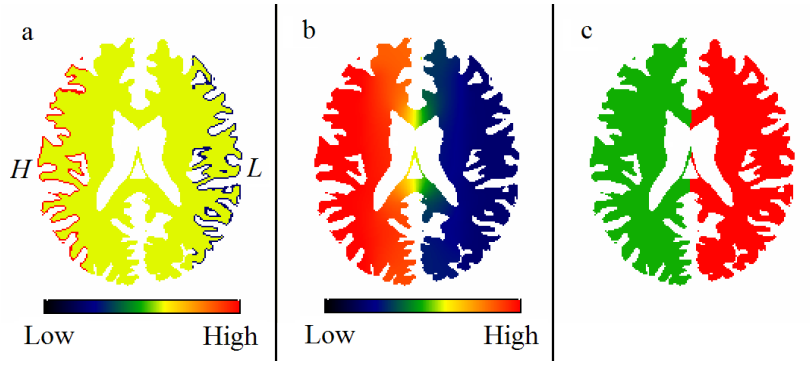

Figure 4.1: Example of implementing the PDE based shape bottlenecks algorithm. (a) initial state, (b) converged state, (c) voxels clustering with respect to IPV.

The PDE based shape bottlenecks algorithm was implemented to detect main shape bottlenecks of brain WM network (corpus callosum, AC and BS) [91], and AC and PC in the whole brain volume (GM$\cup$WM) [69]. This automatic shape bottleneck detection approach requires very simple initialization to define the initial status of the simulated information transmission process. Its implementation is only based on the geometric configuration of the processed object, and no intensity information is needed. Therefore, we can utilize the PDE based shape bottleneck algorithm to automatically detect and cut the connections between the left and right CH, the left and right CB, and BS in MR brain image in the native space.

4.2 Partial volume modeling

Before applying the PDE based shape bottlenecks algorithm to brain hemisphere segmentation, some issues related to PVE need to be concerned. The adjacency areas between CH, CB and BS are very thin CSF area. In MRI, the anatomical connections between CH, CB and BS always merge with the PVE voxels of CSF/GM, so that it is difficult to detect them directly. Fortunately, CH, CB and BS have simple connections in the WM+GM/WM region,

i.e. only BS connected with CH and CB, and no connections between CH and CB. Therefore, before hemisphere segmentation with the PDE based shape bottlenecks algorithm, we can separate CH, CB and BS by applying the PDE based shape bottlenecks algorithm to detect and cut the connections between them in the WM+GM/WM region, then reconstruct their original volumes. Because the PVE between CSF/GM mostly occurs at the boundaries of CH, CB and BS, the region of CSF/GM can be used as the contour to restrict the structure reconstruction (see Fig.4.2). To locate the CSF/GM region, partial volume

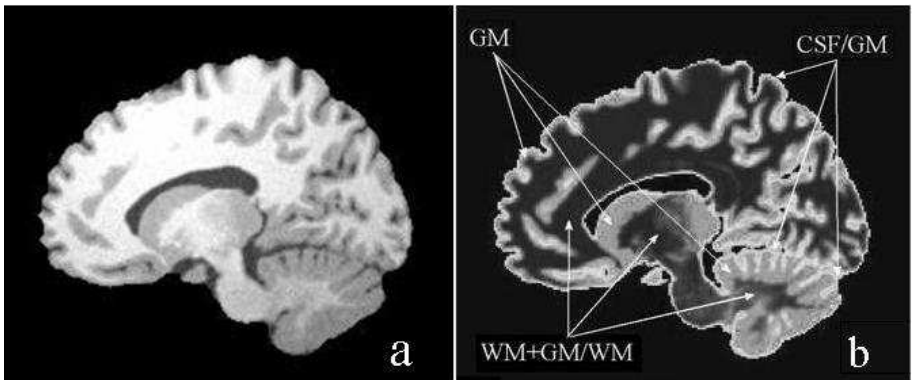

Figure 4.2: Partial volume brain tissue distribution in the sagittal view of a MR brain image. (a) brain volume. (b) partial volume brain tissue labels.

voxel classification is needed. Moreover, after decomposing the brain volume into CH, CB and BS, a part of CSF/GM voxels have to be discarded so that the brain interhemispheric connections are not be covered by CSF contained in the CSF/GM voxels. This statement was demonstrated in [Publication III] and [158]. Nevertheless, over discarding the CSF/GM voxels will cause over removing GM (cortex). The information of tissue proportion of CSF/GM in each voxel is required to control the deleting of CSF/GM voxels.

In this thesis, the partial volume estimation technique developed by Tohka et al. [137] is employed to acquire both the partial volume voxel classification and partial volume tissue fraction. From this partial volume estimation, three images are produced for the three tissue types (CSF, GM or WM) respectively, whose elements reflect the proportion of the corresponding tissue type in each voxel.

4.3 The algorithm of *Adaptive Disconnection*

The *Adaptive Disconnection* algorithm consists of two major steps: brain compartmental decomposition into CH, CB and BS; hemisphere segmentation for CH and CB. The overview of algorithm is illustrated in Fig.2 in [Publication III].

4.3.1 Brain compartmental decomposition

To decompose the brain volume into CH, CB and BS, the WM+GM/WM mask is first segmented to obtain the preliminary segmentation for them. In [91], BS was detected as the shape bottleneck between CH and CB in WM. Whereas the detection result was not considered successful because of the presence of pons in the middle of BS. We conduct the segmentation of the WM+GM/WM mask with a two-step procedure rather than directly treating BS as a shape bottleneck: first CH/CBB segmentation at the midbrain, and then CB/BS segmentation at the cerebellar peduncles. The PDE based shape bottlenecks algorithm is applied twice with different definitions of the information source H and terminal L. In CH/CBB segmentation, H and L are, respectively, located at the top and bottom (superior and inferior) of the WM+GM/WM region. In CB/BS segmentation, H and L are located at the front and back (anterior and posterior) of the CBB part. Both segmentations are completed by classifying the voxels in the produced IPM into two clusters with respect to their IPVs using *k*-means clustering.

The original shapes of the compartments are reconstructed by growing the compartmental seeds towards the region of CSF/GM. Rather than using the intensity information, we define a compartment boundary closing indicator, $P_{boundary}$, to control the growing. For each brain voxel $\mathbf{z}$, the value of $P_{boundary}$ is computed as

$$\forall \mathbf{z} \in \Theta, \quad P_{boundary}(\mathbf{z}) = 2 - \frac{D(\mathbf{z})}{D_{MAX}} - \frac{J(\mathbf{z})}{J_{MAX}}, \tag{4.5}$$

where D and J are the Euclidean distance from $\mathbf{z}$ to the image background and CSF/GM region respectively, and D_{MAX} and J_{MAX} are the maximal values of D and J throughout the brain domain Θ. The value of $P_{boundary}$ represents how close $\mathbf{z}$ is to the compartment boundaries. The growing criterion is as follows. Let $\mathbf{z}_{seed}$ denote a voxel on the boundary of a compartmental seed, and $\mathbf{z}_{neighbor}$ denote one of the 26 neighbors of $\mathbf{z}_{seed}$ that is in the target volume and not labeled. The region, where $\mathbf{z}_{seed}$ is, grows by enclosing $\mathbf{z}_{neighbor}$ if

$$P_{boundary}(\mathbf{z}_{neighbor}) > P_{boundary}(\mathbf{z}_{seed}). \tag{4.6}$$

The growing procedure is implemented iteratively until the whole target volume is filled. More detailed description and method evaluation about this compartmental decomposition is given in [Publication II].

4.3.2 Cerebral and cerebellar hemisphere segmentation

After the compartmental decomposition, all the CSF/GM voxels that are used to restrict the compartment reconstruction remain in the decomposed brain volume. CSF/GM voxels where the percentage of CSF is greater than a threshold value are discarded from the CH or CB volume before the hemisphere segmentation, in order to ensure the hemispheric connections detectable. To select the appropriate threshold value, we assessed the effect of different threshold value (70%, 50%, 30% and 10%) on the subsequent hemisphere segmentation. An example is given in Fig.4.3. Although, the differences between the results il-

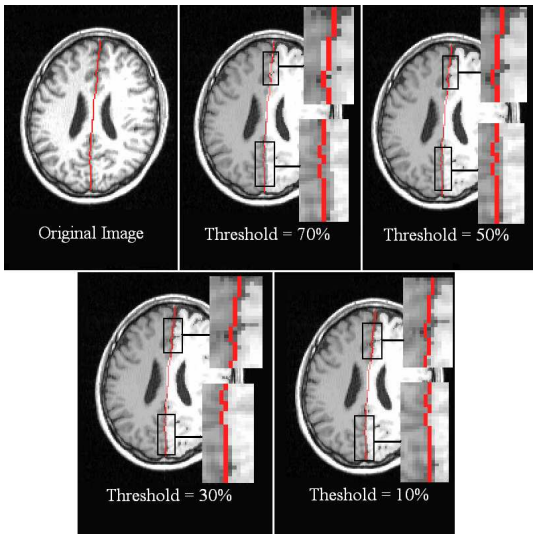

Figure 4.3: Hemisphere segmentation with the *Adaptive Disconnection* method with different threshold value for CSF/GM voxel discarding. The manually identified interhemispheric boundary is illustrated as a red line. The hemisphere segmentation masks, where the left hemisphere is colored grey and the right hemisphere is colored white, are overlapped with the original image.

lustrated in Fig.4.3 are not huge, using threshold = 70% or 50%, to our point of view, did not ensure that the interhemispheric shape bottlenecks can be detected and segmented accurately. There is nearly no visible difference between the segmentation results of 30% and 10%. In this case, using higher threshold value will preserve more GM in the brain volume. Therefore we selected 30%

as the threshold value to remove CSF/GM voxels. The following hemisphere segmentation processes for CH and CB volumes are implemented essentially in the same way as the segmentation of the WM+GM/WM mask. The only difference is that the H and L are the leftmost and rightmost subsets of the CH or CB boundary.

4.4 Method evaluation and results

4.4.1 Segmentation performance evaluation

Evaluating the performances of image segmentation methods is indispensable, since none of them are generally applicable to all images, and different approaches are not equally suitable for a particular application. Image segmentation algorithms can be evaluated either analytically or empirically [157]. The analytical evaluation directly examines and assesses the segmentation algorithms themselves by analyzing their principles and properties. However, not all properties of segmentation algorithms can be obtained by analytical evaluation, since there is no general theory for image segmentation. Furthermore, analytical evaluation often provides only qualitative assessments of algorithms.

The empirical evaluation indirectly judges the segmentation methods by applying them to test images and measuring the quality of segmentation results. Empirical evaluations are mainly used to study the accuracy of segmentation results, which is the primary concern in real applications and is difficult to be tested with analytical evaluation. The segmentation accuracy is the degree to which the segmentation corresponds to the true segmentation, and so the assessment of accuracy of a segmentation requires a reference standard representing the true segmentation, against which it may be compared [145]. Empirical evaluation enables objective comparison between different segmentation algorithms, by generating quantitative accuracy measurements.

The ideal test images for empirical evaluation would reflect the characteristics of segmentation problems encountered in practice. Phantoms can be built and imaged, and incorporated with the imaging system characteristics to increase the realism of the model. This kind of simulated images has an important role to play in quantifying algorithm performance. Nevertheless, such data do not fully reflect imaging characteristics of clinical images, and typically can not reproduce both the normal and pathological anatomical variability observed in clinical data. Therefore, utilizing clinical data is also important for evaluating the segmentation performance on general problems in practice. The reference standard, sometimes is called gold standard or ground truth, is

a correctly or ideally segmented image, which is obtained from the same input image with the evaluated segmentation algorithm. For simulated images, the reference images can be obtained from image generation procedure. For clinical images, manual segmentations generated by trained physicians or radiologists are used as references. In the cases of simulated images of realistic brain anatomy, corresponding reference segmentation is usually acquired based on manual interaction as well.

The accuracy of a segmentation method can be measured as degrees of similarity to the reference segmentation. A simple way to compare the evaluated segmentation against the reference standard is assessing the limits of agreement of volume estimates of the segmented structures [15]. However, volume estimates may be quite similar when the segmented structures are located differently, have different shapes or have different boundaries. Measurements of spatial overlap, such as the Dice [35] and Jaccard [58] similarity coefficients, are often used in practice. Another popular means to evaluate the segmentation accuracy is to measure the degree of discrepancy from the reference segmentation by calculating the percentage of misclassified pixels or voxels (in 3D), considering image segmentation as a pixel/voxel classification process [155]. A number of other alternative metrics have been proposed to obtain the accuracy quantities. An exhaustive review of them is beyond the scope of this thesis. It should be noted that the most appropriate way to carry out the comparison of a segmentation to the reference segmentations is so far unclear [145]. Proper evaluation approach should be selected and adjusted to address the problems confronted in practical experiments.

4.4.2 Experiments and results

The *Adaptive Disconnection* method was compared with the linear registration based MSP extraction algorithm, nonlinear registration based MSS extraction approach (see Section 3.2), and BrainVisa [93] that is perhaps methodologically the closest to it. Empirical evaluation was conducted to achieve the quantitative accuracies of the methods. 10 simulated realistic images from the BrainWeb database [26, 71] and 39 clinical images of healthy brains from the LONI Probabilistic Brain Atlas (LPBA40) database [117] were employed as the test data. The BrainWeb images were of the same simulated realistic subject and only differ in noise and INU levels, so that the evaluation results for this data set can reflect the methods' sensitivities to the image noise and INU. Moreover, the brain hemisphere segmentations with MSP extracted through linear registration existed in the BrainWeb images already, because the images had been correctly affinely registered to Montreal Neurological Institute 305 (MNI305)

stereotaxic space [39]. The LPBA40 data set was used to evaluate the abilities of the methods to process images with practical noise and artifacts, and of real subjects with normally varying morphologies. The segmentation results were quantitatively evaluated against ground-truth manual segmentations. Because, the brain domains to be segmented by the *Adaptive Disconnection* method or BrainVisa were not exactly the same with the domains covered by the employed ground-truth segmentations. Therefore, measurements of spatial overlap, e.g. the Dice [35] and Jaccard [58] similarity coefficients, were not applicable. To address this problem, we designed a new metric to calculate the percentage of misclassified voxels by defining the intersection of the domains covered by the automatic segmentations and ground-truth segmentations as the evaluation domain. The detailed description of the experiments and results were presented in [Publication III].

According to the experimental results, the *Adaptive Disconnection* method performed superiorly to all the other evaluated algorithms. In detail, the *Adaptive Disconnection* method obtained remarkably high accuracies at the occipital lobe where accurate hemisphere segmentation is difficult to be obtained by the linear or nonlinear registration based methods, because of the large normal brain torque. BrainVisa also achieved high accuracies for brain hemisphere segmentation. Nevertheless, its performance to segment the brain hemispheres at some interhemispheric shape bottlenecks, e.g. corpus callosum, was inferior to the *Adaptive Disconnection* method, because its segmentation is blind to the shape bottlenecks themselves. In addition, the *Adaptive Disconnection* method segmented the CH from CBB more precisely than BrainVisa by modeling the compartment boundaries with partial volume information (see Fig.9 in [Publication III]). Furthermore, the stability of the *Adaptive Disconnection* method was reflected by its comparatively stable performance for all the test data. The small variation of the segmentation accuracy for the simulated data set demonstrated that the *Adaptive Disconnection* method is not as sensitive to the noise and INU as other evaluated methods.

In [Publication III], we also applied the *Adaptive Disconnection* method to another clinical T1-weighted MRI data set [72] containing images of 22 healthy controls and 18 never-medicated patients with schizophrenia, named Schizophrenia data set in this thesis. This is to evaluate its performance on images with diagnosis and produced with different imaging parameters from the LPBA40 data set, consequently assess its robustness. There were not ground-truth segmentations for this data set. Thus, we qualitatively evaluated the segmentation results with visual examination. Detailed description of the qualitative evaluation is given in [Publication III] and [158]. From the average cases of segmentation results (see Fig.10 in [Publication III]), it can be seen that the

Adaptive Disconnection method was accurate in decomposing the brain volume into left and right CH, left and right CB, and BS for the Schizophrenia data set.

Besides the experiments proposed in [Publication III], the *Adaptive Disconnection* method was further qualitatively assessed with the International Consortium for Brain Mapping 152 (ICBM152) database [37]. T1-weighted MR images of 152 normal subjects were employed. Excellent brain hemisphere segmentation was also obtained for the entire test data set. In addition, in [Publication II], the quantitative evaluation results of the brain compartmental decomposition algorithm (see Section 4.3.1) enclosed in the *Adaptive Disconnection* method show that the algorithm can separate BS from CH and CB with very high accuracy.

The *Adaptive Disconnection* method obtained excellent performance to segment brain volumes in the images of all the four test databases of different subject groups and with different imaging environments and parameters. This demonstrated that the *Adaptive Disconnection* method is very robust. Furthermore, because the *Adaptive Disconnection* algorithm is fully automatic, we can claim that it is reproducible. The computational complexity and the running time of the algorithm of the proposed method was not seriously concerned in this work, as the former can be overcome with more powerful computational tools and the latter can be dramatically decreased by programming the algorithm in e.g. C language (we programmed the algorithm in Matlab).

Chapter 5

Automatic brain asymmetry analysis

5.1 Introduction

The left and right hemispheres of human brain differ in their anatomy and function. This phenomenon of lateralized difference between the two hemispheres is called brain asymmetry. For anatomical brain asymmetry, the width and volume of the right frontal lobe are often greater than the left, and the width and volume of the left occipital lobe are often larger than the right [13, 44, 77]. These right frontal and left occipital protrusions are known as petalias, which also induce impressions on the inner skull surface. Another prominent geometric distortion of the brain hemispheres, known as Yakovlevian torque, is that the right frontal lobe is torqued forward the left, and the left occipital lobe extends across the midline (over the right occipital lobe) and skews the interhemispheric fissure towards the right [136] (see Fig.5.1). Brain asymmetry is thought to originate from evolutionary, developmental, hereditary, experiential and pathological factors, and it has also been correlated with asymmetrical behavioral traits, such as handedness, auditory perception, motor preferences, and sensory acuity [136].

MRI based brain asymmetry analysis provides methods for computer-assisted diagnosis for mental diseases, e.g. schizophrenia and Alzheimer's disease. By studying the brain asymmetry in groups of healthy controls and patients, the differences between controls and patients can be modeled and objective diagnostic information can be provided to physicians. The brain anatomy analysis approaches introduced in Section 1.2.2 can be applied to analyze brain asymmetry within MRI. Specially, interhemispheric point correspondence needs to be established for the morphometry or surface based shape analysis methods,

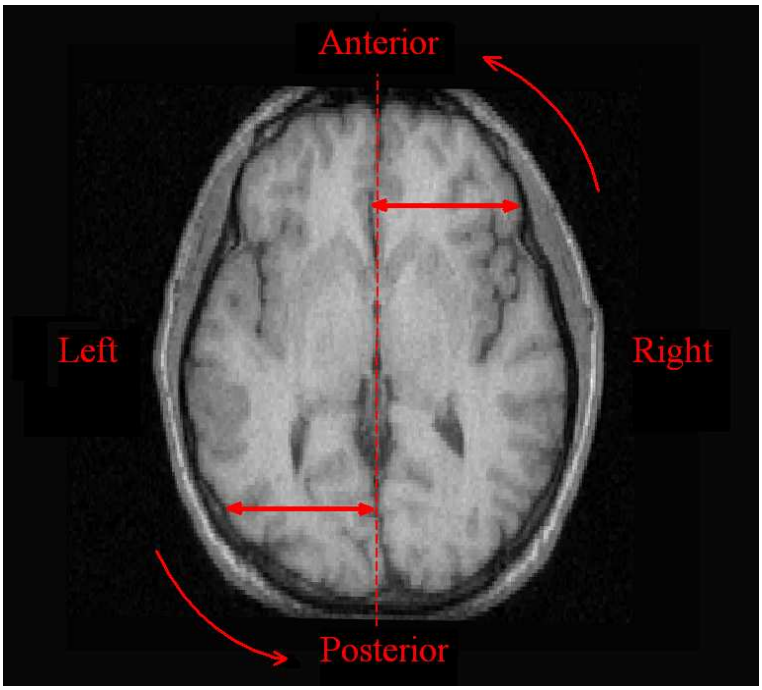

Figure 5.1: Petalia and Yakovlevian torque of human brain.

besides the inter-subject point correspondence. In this chapter, the applications of the *Adaptive Disconnection* method to automate the MRI based studies of brain asymmetry is presented.

5.2 Bilateral volumetric asymmetry analysis

Abnormal volumetric CH asymmetries in schizophrenia have been reported based on manual hemisphere segmentation in MRI (e.g. [12, 13]). In [Publication III], the results of brain hemisphere segmentation with the *Adaptive Disconnection* method of the Schizophrenia data set were utilized to automatically analyze the CH volumetric asymmetry in schizophrenia. Images of two left-handed and one ambidextrous subjects were excluded from this analysis. The analyzed data set thus contained 18 patients (11 males, 7 females) and 19 healthy controls (12 males, 7 females). The difference between the control and patient populations were statistically compared using the nonparametric permutation test [49] in terms of the asymmetry index (AI)

$$AI = \frac{V_R - V_L}{\frac{1}{2}(V_R + V_L)}, \tag{5.1}$$

where V_R and V_L, respectively, are the volumes of the right and left hemispheres. The volume of each cerebral GM or WM hemisphere was computed by integrating the amount of GM or WM contained in the corresponding hemispheric voxels.

The statistical analysis results are presented in Table 1 in [Publication III]. In the case of cerebral GM, for males, mean AI was positive for both patient and healthy groups, and the absolute value of patients' mean AI was much lower than healthy controls'; for females, the sign of patients' mean AI was reversed from healthy controls'. These indicated a reduced cerebral GM volume asymmetry in male patients, and a reversed cerebral GM volume asymmetry in female patients. According to the results of the permutation test, for females, AI in cerebral GM of the patient group had significantly different probability distribution from the healthy group's (p = 0.002). These findings are well in line with the manual segmentation based study reported in [13] and the neurodevelopmental hypothesis of schizophrenia.

5.3 Bilateral shape asymmetry analysis

Volumetric measurements based brain asymmetry analysis is not able to capture the local structural differences between the brain hemispheres. Detailed shape analyses for brain asymmetry are required. Using interhemispheric reflection, VBM was applied to investigate voxel-wise differences between brain hemispheres in tissue density [146] or tissue volume [8, 48, 88]. In [45, 130], DBM was implemented by nonlinearly co-registering the left and right CH with each other for each individual subject. Then the Jacobian determinant of the deformation fields was used to investigate the local interhemispheric shape asymmetry.

To study brain asymmetry with surface based hemispheric shape representations, the vertex-wise interhemispheric and inter-subject correspondences are first established by using stereotaxic volume or surface registration [86, 102, 104, 144]. Next, one hemispheric surfaces is mirrored against MSP and subtracted the opposite surface with respect to the shape measurements at each vertex. Finally, the deviations from zero are analyzed as the asymmetry measurements.

Especially, the method proposed in [104], which is based on the *Adaptive Disconnection* method, was applied to the same Schizophrenia data set used in Section 5.2 to study the local shape asymmetry of CH in schizophrenia. It was found that, in schizophrenia, reduction of shape asymmetry in the superior frontal lobe in females and occipital lobe in males, and increase of shape

asymmetry in the occipital lobe in females.

5.4 Yakovlevian torque analysis

The general MRI brain asymmetry analyses discussed above focus on the bilateral differences between brain hemispheres. As introduced at the beginning of this chapter, besides the bilateral interhemispheric asymmetries, the Yakovlevian torque, which refers to the bending of the interhemispheric fissure, also is a prominent geometric distortion caused by brain asymmetry. Results from the bilateral brain asymmetry analyses can somehow reflect the Yakovlevian torque. However, the quantification of the interhemispheric fissure bending is indirect, and the related geometric interpretation is difficult. To my knowledge, by far, no efforts had been specially spent to analyze this specific prominent geometric distortion itself.

5.4.1 Shape analysis for Yakovlevian torque

In [Publication IV], an automatic shape analysis approach was introduced to analyze the Yakovlevian torque in 3D MRI. In this method, first, the left and right CH are extracted and segmented in the brain images in the native space utilizing the *Adaptive Disconnection* algorithm. For inter-subject comparison, the segmented CH hemisphere volumes are linearly registered into the ICBM152 brain space [37]. Denote the lateral, longitudinal and vertical axes of the image space as X, Y and Z respectively. Next, a curved interhemispheric medial surface S capturing the shape of the interhemispheric fissure is found for each subject by minimizing an Euclidean distance based energy function:

$$x_S(y,z) = \arg\min_x \{ \mid D_l(x,y,z) - D_r(x,y,z) \mid \}. \tag{5.2}$$

where $x_S(y,z)$ is the lateral magnitude of S at (y,z), $D_l(x,y,z)$ and $D_r(x,y,z)$ respectively are the Euclidean distances from a point (x,y,z) on S to the left and right CH hemisphere volumes. The extracted surface S is then mathematically modeled as a polynomial surface, which is a function of its X direction magnitude x_S for each pair of the Y and Z coordinates values.

$$\hat{x}_S(y,z) = \sum_{i=0}^{k} \sum_{j=0}^{i} a_{ij} y^{i-j} z^j, \tag{5.3}$$

where $\hat{x}_S$ is the approximation of x_S determined using least-square fitting, k is the degree of the two-variable polynomial. The process of the interhemispheric surface modeling is illustrated in Fig.1 in [Publication IV].

Curvature features, e.g. principal, Gaussian and mean curvatures, at each point of the fitted interhemispheric surface are calculated based on the 2×2 Hessian matrix

$$\mathcal{H} = \begin{pmatrix} \frac{\partial^2 \hat{x}_S}{\partial y^2} & \frac{\partial^2 \hat{x}_S}{\partial y \partial z} \\ \\ \frac{\partial^2 \hat{x}_S}{\partial y \partial z} & \frac{\partial^2 \hat{x}_S}{\partial z^2} \end{pmatrix}, \tag{5.4}$$

to describe the local bending of the interhemispheric fissure. To describe the regional bending of the interhemispheric fissure, the integrated average value ξ_f of a curvature feature f in a region of interest (ROI) was defined as

$$\xi_f = \frac{\sum_{c_i} \int_{y_i^0}^{y_i^0+2} \int_{z_i^0}^{z_i^0+2} f(y,z) \sqrt{(\frac{\partial \hat{x}_S}{\partial y})^2 + (\frac{\partial \hat{x}_S}{\partial z})^2 + 1}\, dydz}{\sum_{c_i} \int_{y_i^0}^{y_i^0+2} \int_{z_i^0}^{z_i^0+2} \sqrt{(\frac{\partial \hat{x}_S}{\partial y})^2 + (\frac{\partial \hat{x}_S}{\partial z})^2 + 1}\, dydz}, \tag{5.5}$$

where $c_i = [y_i^0, y_i^0 + 2) \times [z_i^0, z_i^0 + 2)$ is a single cell in the projection of the ROI on the mid-sagittal plane in the ICBM152 space; y_i^0 and z_i^0 are the Y and Z coordinates of the origin of c_i; the numerator and denominator, defined with surface integrals, respectively are the total value of f in the ROI and the total area of the ROI.

5.4.2 Application

In [Publication IV], this approach was applied to the Schizophrenia data set described in Section 5.2 to investigate the Yakovlevian torque in schizophrenia.

In this application, the extracted medial interhemispheric surfaces of all subjects were fitted with the polynomial surface with degree of 4, and the selected curvature features were the mean curvature H and curvature in the transverse plane (XY plane) C_{XY}. The points of interest (POIs) were located with the projection of the average volume across all studied CH volumes on MSP of the ICBM152 space. The ROIs were extracted by masking the fitted medial interhemispheric surfaces with the projection of the atlas of LPBA40 [117] on its MSP.

For every subject, the accuracy for automatically detecting the lateral direction of interhemispheric fissure bending with curvature features was evaluated by comparing the bending direction indicated by the signs of ξ_H and $\xi_{C_{XY}}$ in the occipital region against the bending direction manually identified in the transverse slices of the original image. For all the 37 studied subjects, the proposed

method obtained correct detection for 34 subjects with ξ_H and for 36 subjects with $\xi_{C_{XY}}$. Moreover, in all populations, the means of ξ_H and $\xi_{C_{XY}}$ in the occipital region were positive, and their absolute values were always notably greater than their counterparts in the frontal region (see Table 1 [in Publication IV]). This indicates that, in average, the interhemispheric fissure bending of right-handed subject mainly occurs in the occipital region and is laterally rightward. This re-confirms the hypothesis of interhemispheric fissure bending caused by normal Yakovlevian torque [136].

The nonparametric Wilcoxon Rank Sum test [148] was utilized to investigate the statistical difference between controls and patients with schizophrenia with respect to the curvature features at each POI. It was found that for males, POIs with the significant difference between controls and patients were mainly located in the superior frontal region for H and C_{XY}, and in the inferior occipital region for H (see Fig.3 in [Publication IV]).The *t*-test [154] was employed to assess the group difference with respect to the integrated average curvature features in the ROIs corresponding to the frontal and occipital lobes. Significant difference was found between male controls and patients with schizophrenia with respect to the integrated average curvatures ξ_H ($p = 0.0084$) and $\xi_{C_{XY}}$ ($p = 0.036$) in the frontal region. This finding well matches above results of the point-wise analysis.

In addition to the application to the Schizophrenia data set, the proposed automatic shape analysis method was also applied to investigate the Yakovlevian torque of normal brain based on hemisphere segmentation results of the ICBM152 data set with the *Adaptive Disconnection* algorithm (described at the end of Section 4.4.2). Segmented images of 110 right-handed subjects were used. POIs were located with the projection of the ICBM152 average template [37] on its MSP. For each subject, the extracted point-wise mean curvature H was utilized to quantify the local interhemispheric fissure bending, and was regressed against the age and gender factors using a linear model:

$$H \sim b_0 + b_1 AG + b_2 GD + \epsilon, \tag{5.6}$$

where AG and GD respectively are the subject's age and gender, ϵ is the error term. Effects of the coefficients of interest in the linear model (Eq.5.6) were tested using the *t*-test, and were visualized as either a *t*-statistic map (in the case where H is univariate) or a Hotelling's *T* map (in the case where H is multivariate). False discovery rate (FDR) control [10] was employed to correct the multiple comparisons with FDR level = 0.05. The effect map of interhemispheric fissure bending quantified with H is given in Figure 5.2. Main rightward bending can be observed in the occipital, and small portions of the

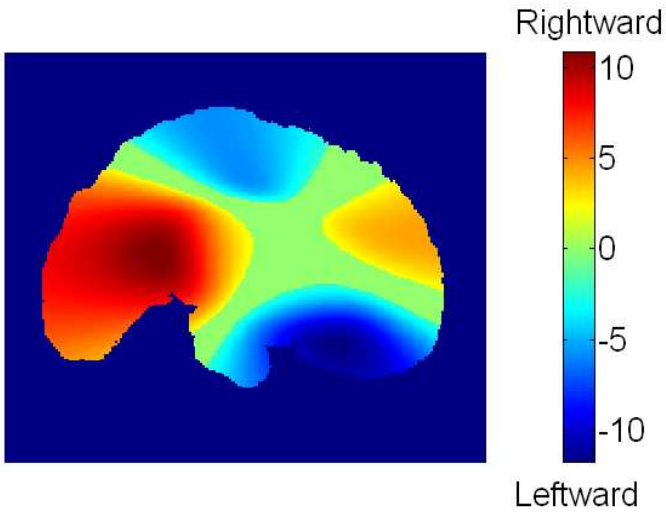

Figure 5.2: Thresholded interhemispheric fissure bending effect (intercept b_0, with $b_1 = b_2 = 0$ in Eq.5.6) map (FDR level = 0.05). Nonsignificant points were set to be zero.

posterior parietal and posterior temporal regions; smaller rightward bending is showed in the anterior frontal region. Main leftward bending is showed in the inferior frontal and inferior temporal regions; smaller leftward bending is found in the superior temporal region. These findings correspond the observations from the Schizophrenia data set, and further confirm the hypothesis about the normal Yakovlevian torque [136]. No significant local age or gender effects were detected.

Chapter 6

Summary of publications

In [Publication I], a novel automatic method to segment the left and right brain hemispheres in 3D MR images was introduced, which is based on the PDE based shape bottlenecks algorithm [91] and a fast and robust partial volume estimation approach [137]. Quantitative evaluation of the method with 10 simulated and qualitative evaluation with 5 real T1-weighted MR images were described. Superiority of the proposed method to the MSP based method was demonstrated.

In [Publication II], a new method was developed to automatically decompose human brain MR images into CH, CB and BS. This method was validated against manual segmentations of 35 T1-weighted MR images. It was demonstrated to be accurate and robust.

In [Publication III], the *Adaptive Disconnection* technique, for automatic segmentation of brain volume into the left and right CH, the left and right CB, and BS in 3D MRI was proposed. Quantitative evaluation of the method and competitive methods with the BrainWeb simulated realistic database [26, 71] and the LPBA40 database [117] was conducted against ground-truth manual segmentations. It performed the best among the investigated methods. A preliminary CH volumetric asymmetry analysis, completed by applying the method to a set of clinical MR images of health controls and never-medicated patients with schizophrenia, was also presented.

In [Publication IV], a novel approach to analyze Yakovlevian torque by quantifying the bending of human brain interhemispheric fissure in 3D MRI was introduced. It was applied to clinical images of healthy controls and never-medicated patients with schizophrenia. The hypothesis of the normal interhemispheric fissure bending (rightward in the occipital region) was quantitatively demonstrated. Significant abnormal interhemispheric fissure bending in male patients was found.

Author’s contribution

The original ideas of [Publication I and IV] were conceived by the author and co-author J. Tohka. The author developed the methods based on the ideas. Based on the general idea of [Publication I], the author developed the new method for brain compartmental decomposition in [Publication II]. In [Publication III], the author combined the techniques developed in [Publication I and II] and further developed the more advanced method. The experiments in all the publications were conducted by the author. All the publications were written by the author, following the comments and suggestions from co-authors. Co-author J. Hirvonen and J. Hietala provided the Schizophrenia data set and counseled on the neurophysiology and anatomy to ensure that the developed methods answered to the correct questions and could be useful in practice.

Chapter 7

Discussion

The development of neuroinformatics promises to extend several important trends in scientific research into the practice of neuroscience. One of the most visible changes is the integration of data into large, international databases [36]. Specially, many brain MRI databases, e.g. [38, 63, 96, 100], have been established, which provide large, demographically balanced and representative samples across wide age range to facilitate the research on human brain structural changes related to aging, development or mental diseases. Under this background, accurate and robust automatic brain image analysis methods are required to analyze the images contained in these databases. To automate the neuroanatomical brain image segmentation is the major bottleneck to automate the brain image analysis [151]. In this thesis, we first developed a novel automatic brain hemisphere segmentation algorithm for 3D MRI: the *Adaptive Disconnection* method. Next, this method was applied to studies of brain structural asymmetry. We also developed an automatic shape analysis method based on the *Adaptive Disconnection* method to study the Yakovlevian torque in 3D MRI. In this chapter, the proposed methods and the related experimental results are discussed.

7.1 Automatic neuroanatomical segmentation

Segmenting the structures or regions of interest in brain MRI is impossible using only the information available in the brain images since there is not sufficient differentiation of features in the intensity space. *A priori* anatomical knowledge of the spatial relationships between different brain structures has to be taken into account. In Section 2.5, we reviewed the atlas deformation based methods [25, 55, 65] and the MAP based statistical methods

[34, 41, 107, 138, 150, 153] for segmenting the cerebral cortical subdivisions and subcortical structures in 3D MRI. The atlas deformation based neuroanatomical segmentation methods directly apply the *a priori* neuroanatomical knowledge contained in pre-delineated atlases to produce the segmentation through nonlinear image registration. The statistical neuroanatomical segmentation algorithms employ training images, which are usually produced by manual segmentation, to learn the prior statistics. We also reviewed the existing brain hemisphere segmentation methods for 3D MRI in Chapter 3. These methods need spatial normalization with standard brain template to address the variations in location and normal brain morphology in different images [30, 54, 64, 68, 79, 94], or with pre-segmented atlas to guide the segmentation [75, 89, 93]. These prerequisites will bring difficulty to applying the methods to databases of specific populations, when the available brain template or pre-segmented images are not suitable for the databases. Additionally, using stereotaxic image registration would make the final segmentation accuracy sensitive to the accuracy of the registration. Differently from the discussed existing techniques, the proposed *Adaptive Disconnection* method does not require the above prerequisites. When the subject orientation in the scanner is given, the method is able to automatically adapt the variation of normal brain morphology in different images without the aid of stereotaxic registration. This gives the method broader applications than the methods using registration, as no specific atlas is required. Although image registration is often needed in quantitative group analyses for spatial normalization or building inter-subject correspondences, producing segmentation that is independent from the registration will avoid introducing potential errors caused by inaccurate registration to subsequent analyses.

Furthermore, the segmentation procedure of most of the existing segmentation approaches uses the intensity information contained in the processed images. Atlas deformation based [25, 55, 65] and registration-morphing-based methods [75, 89] use the intensity information to estimate the optimal registration between the pre-segmented image and the target image. Segmentation-surface-searching based algorithms [79, 94] utilize image intensity based optimization criteria to locate the segmentation surfaces. Compartmental-structure-reconstruction based approaches [30, 54, 64, 68] use the intensity gradients or differences between GM and CSF to guide the structure reconstruction. The segmentation accuracy of the methods depending on image intensity are affected by the presence of image noise and INU. In the *Adaptive Disconnection* method, the intensity information is only employed in image preprocessing, thus it can better tolerate the increase of image noise and INU than other approaches. This has been demonstrated by its stable quantitative evaluation

results for the simulated BrainWeb images [26, 71], which are of the same simulated realistic subject and only differ in levels of noise and INU.

PVE is another important issue needs to be taken into account in automatic neuroanatomical segmentation. For brain hemisphere segmentation, the GM-CSF surface is commonly used to guide the segmentation between the left and right CH and CBB. The existence of PVE always blurs the GM-CSF surface. To our knowledge, this problem is only addressed by CLASP [64] among the existing brain hemisphere segmentation techniques, which reconstructs the cortical hemispheres' surfaces using the skeletonized partial volume CSF surface rather than the GM-CSF interface. In the *Adaptive Disconnection* method, we, for simplicity, directly utilize the regions of partial volume CSF/GM to locate CH, CB and BS boundaries. It has been illustrated that our method can better tolerate the blurring of anatomical compartment boundaries than the techniques that do not model PVE, such as BrainVisa [93]. Nevertheless, a few segmentation errors were still observed near the compartment boundaries when some of the CSF/GM voxels were not exactly located on the boundaries. A potential solution for this problem can be utilizing a skeletonized CSF/GM surface like in CLASP [64] instead of using the entire CSF/GM region to restrict the structure reconstruction. In the *Adaptive Disconnection* method, PVE modeling is also applied to discard a certain amount of CSF/GM voxels in order to make the interhemispheric connections detectable. The improvement for hemisphere segmentation accuracy from this operation has been proved in [Publication III] and [158]. In this work, the threshold value for controling the CSF/GM removing was set to be constant. It is meaningful, in the future, to find an effective approach to adaptively determine the threshold value for different images.

Most of the existing brain hemisphere segmentation methods segment the brain hemispheres in MRI taking the entire hemispheric boundaries into account. In fact, the brain hemispheres are not connected everywhere. Therefore, separating the brain hemisphere volumes by disconnecting them only at the interhemispheric shape bottlenecks would avoid the segmentation errors caused by incorrect detection of the hemispheric boundaries. Both BrainVisa and the *Adaptive Disconnection* method [93] produce the brain hemisphere segmentation in this way. However, the traditional shape bottlenecks algorithm (using morphological erosion and conditional dilation) utilized in BrainVisa conducts the disconnection by breaking the volume shape into separate parts without detecting the shape bottlenecks. As showed in Section 4.4.2, this results in that the segmentation performance of BrainVisa is inferior to the *Adaptive Disconnection* method that detects and cuts the shape bottlenecks using the PDE based shape bottleneck algorithm [91].

The *Adaptive Disconnection* method was quantitatively evaluated with the

BrainWeb simulated image database [26, 71] and the LPBA40 normal clinical scan database [117], and qualitatively tested with the clinical Schizophrenia data set [72] and the ICBM152 normal clinical scan database [37]. Because of the methodological characteristics discussed above, the method obtained high and stable accuracy and excellent performance to segment brain volumes in the images of different subject groups and with different imaging environments and parameters. This proves that the *Adaptive Disconnection* method is very robust. Moreover, due to the reproducibility endowed by the full automaticity, the segmentation errors of the *Adaptive Disconnection* method could be predicted before applying the method so that the subsequent quantitative analysis errors could be predicted or compensated for with some specific postprocesses. For example, in one of the 40 images contained in the LPBA40 database, the longitudinal-distributed INU (the lower part of the image is much darker than the upper part) is extremely severe so that the employed BFC can not correct it to an acceptable level. This will lead to that most of the voxels in CBB that in fact belong to WM would be classified as belonging to GM or CSF. Consequently, the *Adaptive Disconnection* method would not be able to find appropriate seed voxels to reconstruct the structures of CB and BS. This image was excluded in the experiments. This is the only exception we confronted among the over 200 testing images used in this work.

7.2 Brain structural asymmetry studies

The study of human brain asymmetry is a significant research topic in neuroscience, because it can reveal the evolutionary, hereditary, developmental and pathological information of human brain and help early diagnosis for mental diseases and imaging based drug development. Many studies have observed schizophrenia-related reduction or inverse in structural brain asymmetries [13, 105, 119, 124]. However, due to lack of sufficient databases and accurate and robust analysis methods, several investigators failed to replicate the findings in schizophrenia [2, 28, 59, 85], or even obtained conflicting findings [102]. In this thesis, the *Adaptive Disconnection* method was applied to the analyses of CH volumetric [Publication III] and shape asymmetries [104]. We obtained findings that are well in line with the reported manual segmentation based study [13] and the neurodevelopmental hypothesis of brain asymmetry. This demonstrates the ability of the *Adaptive Disconnection* method to automate the brain asymmetry studies.

In addition, an automatic shape analysis approach was developed based on the *Adaptive Disconnection* method to analyze the Yakovlevian torque by quan-

tifying the bending of the interhemispheric fissure. Compared with conventional methods investigating the bilateral structural difference between the brain hemispheres [8, 48, 88, 130, 146], this approach provides morphological interpretations of the Yakovlevian torque that are easier to understand. In the applications of the method to the Schizophrenia data set and the ICBM152 database, the hypothesis of normal interhemispheric fissure bending was confirmed, and abnormal Yakovlevian torque was found in male patients with schizophrenia in the frontal and occipital regions. These results show that this shape analysis approach is applicable for studying Yakovlevian torque for either normal population or patients with mental diseases.

In the experiments of the automatic shape analysis method described in Section 5.4.2, the polynomial surface used to mathematically model the shape of the interhemispheric fissure is selected as the one with degree of 4. Because it is the lowest degree for the curvature features, computed based on the second fundamental form of the polynomial surface, to remain nonlinear properties. It is obvious that more details about the longitudinal shape of the interhemispheric fissure could be preserved when using the polynomial surfaces with higher degree. Nevertheless, these details would bring disturbance for capturing the principal bending tendency of the interhemispheric fissure. Thus the degree of the polynomial surface should not be very large so that it can be smooth enough. To find the optimal degree of the polynomial surface is a meaningful future work to enhance the accuracy of the analysis method. In addition, the employed curvature features were the mean curvature and the curvature in the transverse plane, whose magnitudes and directions can be straightforwardly reflected by their absolute values and signs. In fact, several other curvature features can be simply computed from the second fundamental form of the polynomial surface, e.g. the Gaussian curvature, maximum and minimum curvatures (principal curvatures) and principal directions. Nevertheless, the geometric interpretations of them could be understandable only when they are associated with all the other curvature features. Therefore, simple statistical hypothesis tests are not valid to analyze these features together, more complicated and advanced techniques, e.g. pattern recognition or texture analysis, are needed.

7.3 Other potential applications

The applications of the *Adaptive Disconnection* method are more than to the brain asymmetry studies proposed in this thesis. Brain hemisphere segmentation is often needed for various biomedical and neuroscientific applications, because most of brain structures have the bilateral morphology and functional

lateralization. Brain hemisphere segmentation is also required to separate brain lesions in the left and right brain hemispheres [57], and to view many important brain structures that can be only viewed in the interhemispheric medial surface. The *Adaptive Disconnection* method can be applied to study other smaller brain anatomic sub-divisions as well, e.g. the ventricular system, as long as the segmentation problem can be addressed by the shape bottleneck detection and cutting.

7.4 Conclusions

The objective of this thesis is to develop accurate, robust and automatic brain MRI analysis methods and to validate their abilities to serve large databases based brain researches. According to the results of method evaluations and applications to brain asymmetry studies, it can be concluded that the automatic 3D brain MRI analysis methods developed in this thesis have high accuracy and outstanding robustness, and can facilitate automatic and accurate brain anatomy studies with large brain imaging databases.

Bibliography

[1] O. Acosta, P. Bourgeat, M.A. Zuluaga, J. Fripp, O. Salvado, and S. Ourselin. Automated voxel-based 3D cortical thickness measurement in a combined Lagrangian-Eulerian PDE approach using partial volume maps. *Medical Image Analysis*, 13(5):730–743, 2009.

[2] N.C. Andreasen, J.W. Dennert, S.A. Olsen, and A.R. Damasio. Hemispheric asymmetries and schizophrenia. *Am. J. Psychiatry*, 139:427–430, 1982.

[3] J. Ashburner and K.J. Friston. Nonlinear spatial normalization using basis functions. *Human Brain Mapping*, 7(4):254–266, 1999.

[4] J. Ashburner and K.J. Friston. Voxel-based morphometry - the methods. *NeuroImage*, 11:805–821, 2000.

[5] J. Ashburner and K.J. Friston. Unified segmentation. *Neuroimage*, 26(3):839–851, 2005.

[6] J. Ashburner, C. Hutton, R. Frackowiak, I. Johnsrude, C. Price, and K. Friston. Identifying global anatomical differences: Deformation-based morphometry. *Human Brain Mapping*, 6(5-6):348–357, 1998.

[7] E. Ashton, C. Takahashi, M. Berg, A. Goodman, S. Totterman, and S. Ekholm. Accuracy and reproducibility of manual and semiautomated quantification of MS lesions by MRI. *Journal of Magnetic Resonance Imaging*, 17(3):300–308, 2003.

[8] T.R. Barrick, C.E. Mackay, S. Prima, F. Maes, D. Vandermeulen, T.J. Crow, and N. Roberts. Automatic analysis of cerebral asymmetry: an exploratory study of the relationship between brain torque and planum temporale asymmetry. *NeuroImage*, 24(3):678–91, 2005.

[9] B. Belaroussi, J. Milles, S. Carme, Y.M. Zhu, and H. Benoit-Cattin. Intensity non-uniformity correction in MRI: Existing methods and their validation. *Medical Image Analysis*, 10:234–246, 2006.

[10] Y. Benjamini and Y. Hochberg. Controlling the false discovery rate: a practical and powerful approach to multiple testing. *Journal of the Royal Statistical Society, Series B (Methodological)*, 57(1):125–133, 1995.

[11] J. Bezdek, L. Hall, and L. Clarke. Review of MR image segmentation techniques using pattern recognition. *Med. Physics*, 20(4):1033–1048, 1993.

[12] R.M. Bilder, H. Wu, B. Bogerts, M. Ashtari, D. Robinson, M. Woerner, J.A. Lieberman, and G. Degreef. Cerebral volume asymmetries in schizophrenia and mood disorders: a quantitative magnetic resonance imaging study. *Int. J. Psychophysiol.*, 34:197–205, 1999.

[13] R.M. Bilder, H. Wu, B. Bogerts, G. Degreef, M. Ashtari, J.M. Alvir, P.J. Snyder, and J.A. Lieberman. Absence of regional hemispheric volume asymmetries in first-episode schizophrenia. *Am. J. Psychiatry*, 151(10):1437–47, 1994.

[14] J.G. Bjaalie. Understanding the brain through neuroinformatics. *Front Neurosci.*, 2(1):19–21, 2008.

[15] J.M. Bland and D.G. Altman. Applying the right statistics: Analyses of measurement studies. *Ultrasound Obstet. Gynecol.*, 22:85–93, 2003.

[16] F. Bookstein. Shape and the information in medical images: A decade of the morphometric synthesis. *Computer Vision and Image Understanding*, 66(2):97–118, 1997.

[17] M.E. Brandt, T.P. Bohan, L.A. Kramer, and J.M. Fletcher. Estimation of CSF, white and gray matter volumes in hydrocephalic children using fuzzy clustering of MR images. *Computerized Medical Imaging and Graphics*, 18:25–34, 1994.

[18] M. Brett, I.S. Johnsrude, and A.M. Owen. The problem of functional localization in the human brain. *Nature Reviews Neuroscience*, 3(3):243–249, 2002.

[19] B. Brinkmann, A. Manduca, and R. Robb. Optimized homomorphic unsharp masking for MR grayscale inhomogeneity correction. *IEEE Trans. Med. Imaging*, 17(2):161–171, 1998.

[20] M.E. Brummer. Hough transform detection of the longitudinal fissure in tomographic head images. *IEEE Transactions on Medical Imaging*, 10(1):74–81, 1991.

[21] C.C. Chan. *Analytical Method Validation and Instrument Performance Verification*, pages 17–20. ISBN 9780471259534. John Wiley & Sons, Incorporated, 2004.

[22] H.S. Choi, D.R. Haynor, and Y. Kim. Partial volume tissue classification of multichannel magnetic resonance images - A mixel model. *IEEE Trans. Med. Imag.*, 10(3):395–407, 1991.

[23] G. Christensen, S. Joshi, and M. Miller. Volumetric transformation of brain anatomy. *IEEE Transactions on Medical Imaging*, 16(6):864–877, 1997.

[24] M. Cohen, R. DuBois, and M. Zeineh. Rapid and effective correction of RF inhomogeneity for high field magnetic resonance imaging. *Hum. Brain Mapp.*, 10(4):204–211, 2000.

[25] D.L. Collins, C.J. Holmes, T.M. Peters, and A.C. Evans. Automatic 3D model based neuroanatomical segmentation. *Hum. Brain Mapp.*, 3:190–208, 1995.

[26] D.L. Collins, A.P. Zijdenbos, V. Kollokian, J.G. Sled, N.J. Kabani, C.J. Holmes, and A.C. Evans. Design and construction of a realistic digital brain phantom. *IEEE Trans. Med. Imaging*, 17(3):463–468, 1998.

[27] R.W. Cox. AFNI: software for analysis and visualization of functional magnetic resonance neuroimages. *Comput. Biomed. Res.*, 29:162–173, 1996.

[28] T.J. Crow, N. Colter, C.D. Frith, and E.C. Johnstone. Developmental arrest of cerebral asymmetries in early onset schizophrenia. *Psychiatry Res.*, 29:247–253, 1989.

[29] J. Csernansky, L. Wang, S. Joshi, J. Ratnanather, and M. Miller. Computational anatomy and neuropsychiatric disease: Probabilistic assessment of variation and statistical inference of group difference, hemispheric asymmetry, and time-dependent change. *NeuroImage*, 23:S56–S68, 2004.

[30] A.M. Dale, B. Fischl, and M.I. Sereno. Cortical surface-based analysis: I. segmentation and surface reconstruction. *NeuroImage*, 9:179–194, 1999.

[31] B. Dawant, A. Zijdenbos, and R. Margolin. Correction of intensity variations in MR images for computer-aided tissue classification. *IEEE Trans. Med. Imaging*, 12(4):770–781, 1993.

[32] C. DeCarli, J. Maisog, D.G. Murphy, D. Teichberg, S.I. Rapoport, and B. Horwitz. Method for quantification of brain, ventricular, and subarachnoid CSF volumes from MR images. *J. Comput. Assist. Tomogr.*, 16:274–284, 1992.

[33] M. Desco, J.D. Gispert, S. Reig, A. Santos, J. Pascau, N. Malpica, and P. Garcia-Barreno. Statistical segmentation of multidimensional brain datasets. In *SPIE*, volume 4322, pages 184–193, 2001.

[34] X. Descombes, F. Kruggel, G. Wollny, and H.J. Gertz. An object-based approach for detecting small brain lesions: application to Virchow-Robin spaces. *IEEE Tran. on Medical Img.*, 23(2):246–255, 2004.

[35] L.R. Dice. Measures of the amount of ecologic association between species. *Ecology*, 26(3):297–302, 1945.

[36] P. Eckersley, G.F. Egan, S. Amari, F. Beltrame, R. Bennett, J.G. Bjaalie, T. Dalkara, E. De Schutter, C. Gonzalez, S. Grillner, A. Herz, K.P. Hoffmann, I.P. Jaaskelainen, S.H. Koslow, S.Y. Lee, L. Matthiessen, P.L. Miller, F.M. da Silva, M. Novak, V. Ravindranath, R. Ritz, U. Ruotsalainen, S. Subramaniam, A.W. Toga, S. Usui, J. van Pelt, P. Verschure, D. Willshaw, A. Wrobel, and Y. Tang. Neuroscience data and tool sharing: a legal and policy framework for neuroinformatics. *Neuroinformatics*, 1(2):149–65, 2003.

[37] A. Evans, D. Collins, P. Neelin, D. MacDonald, M. Kamber, and T. Marrett. Three-dimensional correlative imaging: applications in human brain mapping. In M. Huerta, editor, *Functional Neuroimaging: Technical Foundations*, pages 145–162. San Diego: Academic Press, 1994.

[38] A.C. Evans. The NIH MRI study of normal brain development. *Neuroimage*, 30:184–202, 2006.

[39] A.C. Evans, D.L. Collins, S.R. Mills, E.D. Brown, Kelly R.L., and T.M. Peters. 3D statistical neuroanatomical models from 305 MRI volumes.

In *Nuclear Science Symposium and Medical Imaging Conference, IEEE Conference Record (1993)*, 1993.

[40] C. Fennema-Notestine, I.B. Ozyurt, C.P. Clark, S. Morris, A. Bischoff-Grethe, M.W. Bondi, T.L. Jernigan, B. Fischl, F. Segonne, D.W. Shattuck, R.M. Leahy, D.E. Rex, A.W. Toga, K.H. Zou, and G.G. Brown. Quantitative evaluation of automated skull-stripping methods applied to contemporary and legacy images: effects of diagnosis, bias correction, and slice location. *Hum, Brain Mapp.*, 27(2):99–113, 2006.

[41] B. Fischl, D.H. Salat, E. Busa, M. Albert, M. Dieterich, C. Haselgrove, A. van der Kouwe, R. Killiany, D. Kennedy, S. Klaveness, A. Montillo, N. Makris, B. Rosen, and A.M. Dale. Whole brain segmentation: automated labeling of neuroanatomical structures in the human brain. *Neuron*, 33:341–355, 2002.

[42] B. Fischl, M.I. Sereno, and A.M. Dale. Cortical surfacebased analysis. II: Inflation, flattening, and a surfacebased coordinate system. *Neuroimage*, 9:195–207, 1999.

[43] B. Fischl, M.I. Sereno, R.B. Tootell, and A.M. Dale. High-resolution intersubject averaging and a coordinate system for the cortical surface. *Hum. Brain Mapp.*, 8:272–284, 1999.

[44] A.M. Galaburda, M. LeMay, T.L. Kemper, and N. Geschwind. Right-left asymmetrics in the brain. *Science*, 199(4331):852–856, 1978.

[45] C. Gaser, I. Nenadic, B. Buchsbaum, E. Hazlett, and M. Buchsbaum. Deformation-based morphometry and its relation to conventional volumetry of brain lateral ventricles in MRI. *NeuroImage*, 13(6):1140–1145, 2001.

[46] P. Golland, W. Grimson, M. Shenton, and R. Kikinis. Detection and analysis of statistical differences in anatomical shape. *Medical Image Analysis*, 9(1):69–86, 2005.

[47] R. Gonzales and R. Woods. *Digital Image Processing*, page 191. Prentice-Hall, 1992.

[48] C.D. Good, I. Johnsrude, J. Ashburner, R.N.A. Henson, K.J. Friston, and R.S.J. Frackowiak. Cerebral asymmetry and the effects of sex and handedness on brain structure: a voxel-based morphometric analysis of 465 normal adult human brains. *NeuroImage*, 14:685–700, 2001.

[49] P. Good. *Permutation, Parametric and Bootstrap Tests of Hypotheses*. Springer, 3rd edition, 2005.

[50] H. Hahn and H.-O. Peitgen. The skull stripping problem in MRI solved by a single 3D watershed transform. In *MICCAI'00, LNCS 1935*, pages 134–143.

[51] L.O. Hall, A.M. Bensaid, L.P. Clarke, R.P. Velthuizen, M.S. Silbiger, and J.C. Bezdek. A comparison of neural network and fuzzy clustering techniques in segmenting magnetic resonance images of the brain. *IEEE Trans. Neural Networks*, 3:672–682, 1992.

[52] C. Han, T. Hatsukami, and C. Yuan. A multi-scale method for automatic correction of intensity non-uniformity in MR images. *J. Magn. Reson. Imaging*, 13(3):428–436, 2001.

[53] G. Harris, P. Barta, L. Peng, S. Lee, P. Brettschneider, A. Shah, J. Henderer, T. Schlaepfer, and G. Pearlson. MR volume segmentation of gray matter and white matter using manual thresholding: dependence on image brightness. *Am. J. Neuroradiol.*, 15(2):225–230, 1994.

[54] Y. Hata, S. Kobashi, S. Hirano, H. Kitagaki, and E. Mori. Automated segmentation of human brain MR images aided by fuzzy information granulation and fuzzy inference. *IEEE Trans. Syst., Man. Cybern. C*, 30(3):381–395, 2000.

[55] R.A. Heckemann, J.V. Hajnal, P. Aljabar, D. Rueckert, and A. Hammers. Automatic anatomical brain MRI segmentation combining label propagation and decision fusion. *NeuroImage*, 33(1):115–126, 2006.

[56] K. Held, E. R. Kops, B. J. Krause, W. M. Wells III, R. Kikinis, and H.-W. M-Gartner. Markov random field segmentation of brain MR images. *IEEE Trans. Med. Imag.*, 16:878–886, 1997.

[57] S.A. Hojjatoleslami and F Kruggel. Segmentation of large brain lesions. *IEEE Trans Med Imaging*, 20(7):666–669, 2001.

[58] P. Jaccard. The distribution of flora in the alpine zone. *New Phytologist*, 11:37–50, 1912.

[59] T.L. Jernigan, L.M. Zatz, J.A. Moses Jr., and J.P. Cardellino. Computed tomography in schizophrenics and normal volunteers: II. cranial asymmetry. *Arch. Gen. Psychiatry*, 39:771–773, 1982.

[60] B. Johnston, M. Atkins, B. Mackiewich, and M. Anderson. Segmentation of multiple sclerosis lesions in intensity corrected multispectral MRI. *IEEE Trans. Med. Imaging*, 15(2):154–169, 1996.

[61] M. Joliot and B.M. Mazoyer. Three-dimensional segmentation and interpolation of magnetic resonance brain images. *IEEE Trans. Med. Imag.*, 12(2):269–277, 1993.

[62] S.E. Jones, B.R. Buchbinder, and I. Aharon. Three-dimensional mapping of cortical thickness using Laplace's equation. *Hum. Brain Mapp.*, 11:12–32, 2000.

[63] M.J. Kempton, J.R Geddes, U. Ettinger, S.C. Williams, and P.M. Grasby. Meta-analysis, database, and meta-regression of 98 structural imaging studies in bipolar disorder. *Archives of General Psychiatry*, 65:1017–1032, 2008.

[64] J.S. Kim, V. Singh, J.K. Lee, J. Lerch, Y. Ad-Dab'bagh, D. MacDonald, J.M. Lee, S.I. Kim, and A.C. Evans. Automated 3-D extraction and evaluation of the inner and outer cortical surfaces using a Laplacian map and partial volume effect classification. *NeuroImage*, 27:210–221, 2005.

[65] A. Klein, B. Mensh, S. Ghosh, J. Tourville, and J. Hirsch. Mindboggle: automated brain labeling with multiple atlases. *BMC Med. Imaging*, 5(1), 2005.

[66] J. Koikkalainena, J. Hirvonen, M. Nymanb, J. Lötjönen, J. Hietala, and U. Ruotsalainen. Shape variability of the human striatumłeffects of age and gender. *NeuroImage*, 34(1):85–93, 2007.

[67] A. Koivula, J. Alakuijala, and O. Tervonen. Image feature based automatic correction of low-frequency spatial intensity variations in MR images. *Magn. Reson. Imaging*, 15(10):1167–1175, 1997.

[68] N. Krigeskorte and R. Goebel. An efficient algorithm for topologically correct segmentation of the cortical sheet in anatomical MR volumes. *NeuroImage*, 14(2):329–346, 2001.

[69] F. Kruggel and D. von Cramon. Alignment of magnetic resonance brain datasets with the stereotactical coordinate system. *Med. Image Anal.*, 3:175–185, 1999.

[70] A. Kundu. Local segmentation of biomedical images. *Computerized Medical Imaging and Graphics*, 14:173–183, 1990.

[71] R.-S. Kwan, A.C. Evans, and G.B. Pike. MRI simulation based evaluation and classifications methods. *IEEE Trans. Med. Imaging*, 18(11):1085–1097, 1999.

[72] M.P. Laakso, J. Tiihonen, E. Syv$\ddot{a}$lahti, H. Vilkman, A. Laakso, B. Alakare, V. R$\ddot{a}$kk$\ddot{o}$l$\ddot{a}$inen, R.K. Salokangas, E. Koivisto, and J. Hietala. A morphometric MRI study of the hippocampus in first-episode, neuroleptic-naive schizophrenia. *Schizophr Res.*, 50(1-2):3–7, 2001.

[73] S.-H. Lai and M. Fang. A new variational shape-from-orientation approach to correcting intensity inhomogeneities in magnetic resonance images. *Med. Image Anal.*, 3(4):409–424, 1999.

[74] D.H. Laidlaw, K.W. Fleischer, and A.H. Barr. Partial-volume Bayesian classification of material mixtures in MR volume data using voxel histograms. *IEEE Transactions on Medical Imaging*, 17(1):74–86, 1998.

[75] J. Larsson. *Imaging vision: functional mapping of intermediate visual processes in man, PhD Thesis*. ISBN: 91-7349-090-3. Karolinska Institutet, Stockholm, Sweden, 2001.

[76] J.-M. Lee, S. Kim, D. Jang, T. Ha, J.-J. Kim, I. Kim, J. Kwon, and S. Kim. Deformable model with surface registration for hippocampal shape deformity analysis in schizophrenia. *NeuroImage*, 22(2):831–840, 2004.

[77] M. LeMay. Morphological cerebral asymmetries of modern man, fossil man and non-human primate. *Ann. N. Y. Acad. Sci.*, 280:349–369, 1976.

[78] J. Levitt, C. Westin, P. Nestor, R. Estepar, C. Dickey, M. Voglmaier, L. Seidman, R. Kikinis, F. Jolesz, R. McCarley, and M. Shenton. Shape of caudate nucleus and its cognitive correlates in neuroleptic-naive schizotypal personality disorder. *Biological Psychiatry*, 55(2):177–184, 2004.

[79] L.C. Liang, K. Relly, R.P. Woods, and D.A. Rottenberg. Automatic segmentation of left and right cerebral hemispheres from MRI brain volumes using the graph cuts algorithm. *NeuroImage*, 34(3):1160–1170, 2006.

[80] A.W.C. Liew and H. Yan. An adaptive spatial fuzzy clustering algorithm for MR image segmentation. *IEEE Trans. Med. Imag.*, 22(9):1063–1075, 2003.

[81] B. Likar, M. Viergever, and F. Pernus. Retrospective correction of MR intensity in MR inhomogeneity by information minimization. *IEEE Trans. Med. Imaging*, 20(12):1398–1410, 2001.

[82] K.O. Lim and A. Pfefferbaum. Segmentation of MR brain images into cerebrospinal fluid spaces, white and gray matter. *Journal of Computational Assistant Tomography*, 13(4):588–593, 1989.

[83] F.-H. Lin, Y.-J. Chen, J. Belliveau, and L. Wald. A wavelet-based approximation of surface coil sensitivity profiles for correction of image intensity inhomogeneity and parallel imaging reconstruction. *Hum. Brain Mapp.*, 19(2):96–111, 2003.

[84] Y. Liu, R.T. Collins, and W.E. Rothfus. Robust midsagittal plane extraction from normal and pathological 3D neuroradiology images. *IEEE Transactions on Medical Imaging*, 20(3):175–192, 2001.

[85] D.J. Luchins and H.Y. Meltzer. A blind, controlled study of occipital cerebral asymmetry in schizophrenia. *Psychiatry Res.*, 10:87–95, 1983.

[86] O.C. Lyttelton, S. Karama, Y. Ad-Dab'bagh, R.J. Zatorre, F. Carbonell, K. Worsley, and A.C. Evans. Positional and surface area asymmetry of the human cerebral cortex. *NeuroImage*, 46(4):895–903, 2009.

[87] C.M. Ma and S.Y. Wan. A medial-surface oriented 3-D two-subfield thinning algorithm. *Pattern Recogn. Lett.*, 22:1439–1446, 2001.

[88] C.E. Mackay, T.R. Barrick, N. Roberts, L.E. DeLisi, F. Maes, D. Vandermeulen, and T.J. Crow. Application of a new image analysis technique to the study of brain asymmetry in schizophrenia. *Psychiatry Res. NeuroImaging*, 124(1):25–35, 2003.

[89] F. Maes, K. Van Leemput, L. DeLisi, D. Vandermeulen, and P. Suetens. Quantification of cerebral grey and white matter asymmetry from MRI. *Lecture Notes in Computer Science*, 1679:348–357, 1999.

[90] J.-F. Mangin. Entropy minimization for automatic correction of intensity nonuniformity. In *IEEE Workshop on Mathematical Methods in Biomedical Image Analysis (MMBIA'00)*, pages 162–169, 2000.

[91] J.-F. Mangin, J. Régis, and V. Frouin. Shape bottlenecks and conservative flow systems. In *IEEE Work. MMBIA*, pages 319–328, San Francisco, CA, 1996.

[92] J.-F. Mangin, D. Rivière, A. Cachia, E. Duchesnay, Y. Cointepas, D. Papadopoulos-Orfanos, D. Collins, A. Evans, and J. Règis. Object-based morphometry of the cerebral cortex. *IEEE Transactions on Medical Imaging*, 23(8):968–982, 2004.

[93] J.-F. Mangin, D. Rivière, A. Cachia, E. Duchesnay, Y. Cointepas, D. Papadopoulos-Orfanos, P. Scifo, T. Ochiai, F. Brunelle, and J. Régis. A framework to study the cortical folding patterns. *NeuroImage*, 23:129–138, 2004.

[94] P. Marais and J.M. Brady. Detecting the brain surface in sparse MRI using boundary models. *Medical Image Analysis*, 4:283–302, 2000.

[95] P. Marais, R. Guillemaud, M. Sakuma, A. Zisserman, and M. Brady. Visualising cerebral asymmetry. In *Proc. of the 4th International Conference on Visualization in Biomedical Computing VBC'96*, pages 411–416, London, UK, 1996.

[96] D.S. Marcus, T.H. Wang, J. Parker, J.G. Csernansky, J.C. Morris, and R.L. Buckner. Open access series of imaging studies (OASIS): cross-sectional MRI data in young, middle aged, nondemented, and demented older adults. *J Cogn Neurosci*, 19(9):1498–1507, 2007.

[97] C. Meyer, P. Bland, and J. Pipe. Retrospective correction of intensity inhomogeneities in MRI. *IEEE Trans. Med. Imaging*, 14(1):36–41, 1995.

[98] J. Milles, Y. Zhu, N. Chen, L. Panych, G. Gimenez, and C. Guttmann. MRI intensity nonuniformity correction using simultaneously spatial and gray-level histogram information. In *SPIE Medical Imaging*, pages 734–742, 2004.

[99] J. Montagnat, H. Delingette, and N. Ayache. A review of deformable surfaces: topology, geometry and deformation. *Image Vision Comput.*, 19(14):1023–1040, 2001.

[100] S.G. Mueller, M.W. Weiner, L.J. Thal, R.C. Petersen, C. Jack, W. Jagust, J.Q. Trojanowski, A.W. Toga, and L. Beckett. The Alzheimer's Disease Neuroimaging Initiative. *Neuroimaging Clin N Am*, 15(4):869–877, 2005.

[101] P. Narayana and A. Borthakur. Effect of radio frequency inhomogeneity correction on the reproducibility of intra-cranial volumes using MR image data. *Magnet. Reson. Med.*, 33(3):396–400, 1995.

[102] K.L. Narr, R.M. Bilder, E. Luders, Thompson P.M., R.P. Woods, D. Robinson, P.R. Szeszko, T. Dimtcheva, M. Gurbani, and A.W. Toga. Asymmetries of cortical shape: Effects of handedness, sex and schizophrenia. *Neuroimage*, 34(3):939–48, 2007.

[103] A. Noe and J. Gee. Partial volume segmentation of cerebral MRI scans with mixture model clustering. In *Proc. of Information Processing in Medical Imaging, 17th International Conference. LNCS 2082 IPMI*, pages 423–430. Springer-verlag, Berlin/Heidelberg, 2001.

[104] A. Pepe. *Automatic shape asymmetry analysis of human cerebral hemispheres in schizophrenia based on MRI*. Master of Science Thesis, Department of Signal Processing, Tampere Univeristy of Technology, Finland, 2008.

[105] R.G. Petty. Structural asymmetries of the human brain and their disturbance in schizophrenia. *Schizophrenia Bulletin*, 25:121–139, 1999.

[106] D. Pham and J. Prince. Adaptive fuzzy segmentation of magnetic resonance images. *IEEE Trans. Med. Imag.*, 18:737–752, 1999.

[107] K.M. Pohl, J. Fisher, R. Kikinis, W.E.L. Grimson, and W.M. Wells. A Bayesian model for joint segmentation and registration. *NeuroImage*, 31:228–239, 2006.

[108] S. Prima, S. Ourselin, and N. Ayache. Computation of the mid-sagittal plane in 3D brain images. *IEEE Transactions on Medical Imaging*, 21(2):122–138, 2002.

[109] J.C. Rajapakse, J.N. Giedd, and J.L. Rapoport. Statistical approach to segmentation of single-channel cerebral MR images. *IEEE Trans. Med. Imag.*, 16(2):176–186, 1997.

[110] K.R. Rocha, A.J. Jr. Yezzi, and J.L. Prince. A hybrid Eulerian-Lagrangian approach for thickness, correspondence, and gridding of annular tissues. *IEEE Trans Image Process.*, 16(3):636–648, 2007.

[111] S. Ruan, J.H. Xue, J. Fadili, D. Bloyet, and C. Jaggi. Brain tissue classification of magnetic resonance images using partial volume modeling. *IEEE Trans. Med. Imaging*, 19(12):1179–1187, 2000.

[112] J.M. Sanches, J.C. Nascimento, and Marques J.S. Medical image noise reduction using the Sylvester-Lyapunov equation. *IEEE Trans. Image Process.*, 17(9):1522–1539, 2008.

[113] S. Sandor and R. Leahy. Surface-based labeling of cortical anatomy using a deformable database. *IEEE Trans. Med. Imag.*, 16:41–54, 1997.

[114] P. Santago and H.D. Gage. Quantification of MR brain images by mixture density and partial volume modeling. *IEEE Trans. Med. Imag.*, 12(3):566–574, 1993.

[115] T. Schormann and K. Zilles. Three-dimensional linear and nonlinear transformations: an integration of light microscopical and MRI data. *Hum. Brain Mapp.*, 6:339–347, 1998.

[116] F. Segonne, A.M. Dale, E. Busa, M Glessner, D Salat, H.K. Hahn, and B. Fischl. A hybrid approach to the skull stripping problem in MRI. *Neuroimage*, 22:1060–1075, 2004.

[117] D.W. Shattuck, M. Mirza, V. Adisetiyo, C Hojatkashani, G Salamon, K.L. Narr, R.A. Poldrack, R.M. Bilder, and A.W. Toga. Construction of a 3D probabilistic atlas of human cortical structures. *NeuroImage*, 39:1064–1080, 2008.

[118] D.W. Shattuck, S.R. Sandor-Leahy, K.A. Schaper, D.A. Rottenberg, and R.M. Leahy. Magnetic resonance image tissue classification using a partial volume model. *NeuroImage*, 13(5):856–876, 2001.

[119] M.E. Shenton, C.C. Dickey, M. Frumin, and R.W. McCarley. A review of MRI findings in schizophrenia. *Schizophr Res.*, 49(1-2):1–52, 2001.

[120] J. Sled, A. Zijdenbos, and A. Evans. A nonparametric method for automatic correction of intensity nonuniformity in MRI data. *IEEE Trans. Med. Imaging*, 17(1):87–97, 1998.

[121] J. G. Sled and G. B. Pike. Understanding intensity nonuniformity in MRI. In *Medical Image Computing and Computer-Assisted Intervention (MICCAI'98), Lecture Notes in Computer Science (W. M. Wells, A. C. F. Colchester, and S. Delp, Eds.)*, volume 1496, pages 614–622, 1998.

[122] S.M. Smith. Fast robust automated brain extraction. *Hum. Brain Mapp.*, 17:143–155, 2002.

[123] E. Solanas and J.-P. Thiran. Exploiting voxel correlation for automated MRI bias field correction by conditional entropy minimization. In *International Conference on Medical Image Computing and Computer-Assisted Intervention (MICCAI'01)*, pages 1220–1221, 2001.

[124] I. Sommer, N. Ramsey, R. Kahn, A. Aleman, and A. Bouma. Handedness, language lateralisation and anatomical asymmetry in schizophrenia: meta-analysis. *British Journal of Psychiatry*, 178:344–351, 2001.

[125] M. Styner, C. Brechbuhler, G. Szekely, and G. Gerig. Parametric estimate of intensity inhomogeneities applied to MRI. *IEEE Trans. Med. Imaging*, 19(3):153–165, 2000.

[126] C. Sun and J. Sherrah. 3D symmetry detection using the extended Gaussian image. *IEEE Trans. Pattern Anal. Mach. Intell.*, 19(2):164–168, 1997.

[127] H. Suzuki and J. Toriwaki. Automatic segmentation of head MRI images by knowledge guided thresholding. *Computerized Medical Imaging and Graphics*, 15(4):233–240, 1991.

[128] J. Talairach and P. Tournoux. *Co-Planar Stereotaxic Atlas of the Human Brain*. Thieme Medical Publishers, New York, 1988.

[129] R. Tepest, L. Wang, M. Miller, P. Falkai, and J. Csernansky. Hippocampal deformities in the unaffected siblings of schizophrenia subjects. *Biological Psychiatry*, 54(11):1234–1240, 2003.

[130] J.-P. Thirion, S. Prima, G. Subsol, and N. Roberts. Statistical analysis of normal and abnormal dissymmetry in volumetric medical images. *Med. Image Anal.*, 4:111–121, 2000.

[131] P.M. Thompson, M. Mega, and A.W. Toga. Detection, visualization and animation of abnormal anatomic structure with a deformable probabilistic brain atlas based on random vector field transformations. *Medical Image Analysis*, 1(4):271–294, 1997.

[132] P.M. Thompson and A.W. Toga. In I. Bankman, editor, *Handbook of Medical Imaging: Processing and Analysis*, pages 569–600. Academic, San Diego, 2000.

[133] P.M. Thompson and A.W. Toga. A framework for computational anatomy. *Computing and Visualization in Science*, 5(1):13–34, 2002.

[134] P.M. Thompson, R.P. Woods, M.S. Mega, and A.W. Toga. Mathematical/computational challenges in creating deformable and probabilistic atlases of the human brain. *Hum. Brain Mapp.*, 9:81–92, 2000.

[135] M. Tincher, R. Meyer, R. Gupta, and W. Williams. Polynomial modeling and reduction of RF body coil spatial inhomogeneity in MRI. *IEEE Trans. Med. Imaging*, 12(2):361–365, 1993.

[136] A.W. Toga and P.M. Thompson. Mapping brain asymmetry. *Nature Reviews Neuroscience*, 4(1):37–48, 2003.

[137] J. Tohka, A. Zijdenbos, and A.C. Evans. Fast and robust parameter estimation for statistical partial volume models in brain MRI. *NeuroImage*, 23(1):84–97, 2004.

[138] Z. Tu, K.L. Narr, P. Dollar, I. Dinov, P. Thompson, and A. Toga. Brain anatomical structure segmentation by hybrid discriminative/generative models. *IEEE Trans. Med. Imaging*, 27(4):495–508, 2008.

[139] K. Van Leemput, F. Maes, D. Vandermeulen, and P. Suetens. Automated model-based bias field correction of MR images of the brain. *IEEE Trans. Med. Imag.*, 18(10):885–896, 1999.

[140] K. Van Leemput, F. Maes, D. Vandermeulen, and P. Suetens. Automated model-based tissue classification of MR images of the brain. *IEEE Trans. Med. Imag.*, 18(10):897–908, 1999.

[141] E. Vokurka, N. Thacker, and A. Jackson. A fast model independent method for automatic correction of intensity nonuniformity in MRI data. *J. Magn. Reson. Imaging*, 10(4):550–562, 1999.

[142] U. Vovk, F. Pernus, and B. Likar. MRI intensity inhomogeneity correction by combining intensity and spatial information. *Phys. Med. Biol.*, 49(17):4119–4133, 2004.

[143] L. Wald, L. Carvajal, S. Moyher, S. Nelson, P. Grant, A. Barkovich, and D. Vigneron. Phased array detectors and an automated intensity-correction algorithm for high-resolution MR imaging of the human brain. *Magnet. Reson. Med.*, 34(3):433–439, 1995.

[144] L. Wang, S. Joshi, M. Miller, and J. Csernansky. Statistical analysis of hippocampal asymmetry in schizophrenia. *NeuroImage*, 14(3):531–545, 2001.

[145] S.K. Warfield, K.H. Zou, and W.M. Wells. Simultaneous truth and performance level estimation (STAPLE): An algorithm for the validation of image segmentation. *IEEE Trans. Med. Imag.*, 23(7):903–921, 2004.

[146] K.E. Watkins, Lerch-J.P. Paus, T., A. Zidjenbos, D.L. Collins, P. Neelin, J. Taylor, K.J. Worsley, and A.C. Evans. Structural asymmetries in the human brain: a voxel-based statistical analysis of 142 MRI scans. *Cereb. Cortex*, 11:868–877, 2001.

[147] W.M. Wells III, W.E.L. Grimson, R. Kikinis, and F.A. Jolesz. Adaptive segmentation of MRI data. *IEEE Trans. Med. Imag.*, 15:429–442, 1996.

[148] F. Wilcoxon. Individual comparisons by ranking methods. *Biometrics*, 1:80–83, 1945.

[149] R.P. Woods, S.T. Grafton, Watson J.D., N.L. Sicotte, and J.C. Mazziotta. Automated image registration: II. Intersubject validation of linear and nonlinear models. *J. Comput. Assist. Tomogr.*, 22:153–165, 1998.

[150] M.W. Woolrich and T.E. Behrens. Variational Bayes inference of spatial mixture models for segmentation. *IEEE Trans. on Medical Imaging*, 2(10):1380–1391, 2006.

[151] A.J. Worth, N. Makris, V.S. Caviness, and D.N. Kennedy. Neuroanatomical segmentation in MRI: Technological objectives. *International Journal of Pattern Recognition and Artificial Intelligence (IJPRAI)*, 11(8):1161–1187, 1997.

[152] J. Xu, S. Kobayashi, S. Yamaguchi, K. Iijima, K. Okada, and K. Yamashita. Gender effects on age-related changes in brain structure. *American Journal of Neuroradiology*, 21(1):112–118, 2000.

[153] J. Yang, L.H. Staib, and J.S. Duncan. Neighbor-constrained segmentation with level set based 3D deformable models. *IEEE Trans. on Medical Imaging*, 23(8):940–948, 2004.

[154] X.S. Yang. *Applied Engineering Mathematics*, pages 299–303. ISBN 978-1-904602-56-9. Cambridge International Science Publishing, 2008.

[155] W.A. Yasnoff, J.K. Mui, and J.M. Bacus. Error measures for scene segmentation. *Pattern Recognition*, 9:217–231, 1977.

[156] A. Yezzi and J. Prince. An Eulerian PDE approach for computing tissue thickness. *IEEE Trans Med Imaging*, 22(10):1332–1339, 2003.

[157] Y.J. Zhang. survey on evaluation methods for image segmentation. *Pattern Recognition*, 29(8):1335–1346, 1996.

[158] L. Zhao, J. Tohka, J. Hirvonen, J. Hietala, and U. Ruotsalainen. Evaluation of a novel brain hemisphere segmentation method using MR images of schizophrenics and healthy controls. In *Proc. of Finnish Signal Processing Symposium (FINSIG'07)*, ISBN 978-951-42-8546-2, Oulu, Finland, 2007.

[159] L. Zhou, Y. Zhu, C. Bergot, A.-M. Laval-Jeantet, V. Bousson, J.-D. Laredo, and M. Laval-Jeantet. A method of radio-frequency inhomogeneity correction for brain tissue segmentation in MRI. *Comput. Med. Imag. Grap.*, 25(5):379–389, 2001.

[160] A. Zijdenbos, B. Dawant, and R Margolin. Intensity correction and its effect on measurement variability in MRI. In *International Symposium and Exhibition on Computer Assisted Radiology and Surgery (CARS'95)*, pages 216–221, 1995.

Publications

Publication I

L. Zhao, J. Tohka, and U. Ruotsalainen. Accurate 3D left-right brain hemisphere segmentation in MR images based on shape bottlenecks and partial volume estimation. In B.K. Ersboll and K.S. Pedersen, editors, *Proc. of 15th Scandinavian Conference on Image Analysis, SCIA07, Lecture Notes in Computer Science 4522*, pages 581 - 590, Aalborg, Denmark, Springer Verlag, June 2007.

Publication II

L. Zhao and J. Tohka. Automatic compartmental decomposition for 3D MR images of human brain. *Proc. of 30th Annual International Conference of the IEEE Engineering in Medicine and Biology Society, EMBC08*, pages 3888-3891, Vancouver, Canada, August 2008.

Publication III

L. Zhao, U. Ruotsalainen, J. Hirvonen, J. Hietala and J. Tohka. Automatic cerebral and cerebellar hemisphere segmentation in 3D MRI: adaptive disconnection algorithm. *Medical Image Analysis*, volume 14, number 3, pages 360 - 372, 2010.

Publication IV

L. Zhao, J. Hietala and J. Tohka. Shape analysis of human brain interhemispheric fissure bending in MRI. *Proc. of 12th International Conference on Medical Image Computing and Computer Assisted Intervention, MICCAI09, Lecture Notes in Computer Science 5762*, pages 216 - 223, London, United Kingdom, Springer Verlag, September 2009.